



# Development of a PV-Wind hybrid system in Pserimos islet

---





Title: *PV-Wind hybrid system installation located in Pserimos islet targeting to the electricity supply of Cos and Calymnos islands*

Author: *Karatzas Stylianos*  
*MSc Energy science*  
*Student number-4122100*

Email: [s.karatzas@students.uu.nl](mailto:s.karatzas@students.uu.nl)  
[k159713@hotmail.com](mailto:k159713@hotmail.com)

University: *Utrecht University*  
*Department of Geosciences*  
*Boedapestlaan 6*  
*3524 CD Utrecht*  
*The Netherlands*

Supervision: *Dr. Wilfried Van Sark ([w.q.j.h.m.vansark@uu.nl](mailto:w.q.j.h.m.vansark@uu.nl))*  
*Dr. Petros Axaopoulos ([pax@teiath.gr](mailto:pax@teiath.gr))*

*September 2015*



## Disclaimer

This material is based upon work supported by Utrecht University. Any opinions, findings or recommendations are those of the authors and do not reflect the views of Utrecht University, its employees or its administration.

## Acknowledgements

I would like to express my gratitude to Dr. Wilfried Van Sark, for giving me the opportunity to develop a Thesis topic based on a subject that it always intrigued me. Additionally, I would like to thank both Dr. Wilfried Van Sark and Dr. Petros Axaopoulos for the contribution and the patient guidance that they showed until the end of this project, solving my more than many questions. I could never forget also Mr. Christos Tsekouras, who was the person that provide me with the idea of this topic, therefore I would like to say a big thank you to him as well. Moreover, special thanks to Dr. Giannikos (Electricity authority of Cos) and Dr. Kostas Lagouvardos (National Observatory of Greece) for providing me all the needed data for the completion of this Thesis. Last but not least, I would like to thank my parents for their support and encouragement thorough my studies.

## Abstract

On the remote islet of Pserimos, which is located on the southern Greek Aegean sea a hybrid system is planned to be installed targeting to cover a share of the electricity needs of two neighbor islands, Cos and Calymnos. The transfer of the produced electricity will be achieved with the use of submarine cables, which will be linked with Cos and Calymnos common local grid, since both islands are already cabled with each other. The hybrid system will be consisted of Photovoltaic units and wind turbines, targeting towards to the substitution of the existed fossil fueled power plants with green renewable energy.

The aim of this Master Thesis is to perform a data analysis based on the wind and irradiation conditions that prevail on Pserimos, targeting to the prediction of the electricity production that will be gained from hybrid's system installation. Moreover, a geographical research of the islet was performed revealing the most favorable surface positions for the units placement, that will lead to increased electricity output. Furthermore, a monthly comparison between the electricity demand of Cos and Calymnos and the produced electricity obtained from Pserimos was investigated, in order to estimate the system's supplied covering share.

The study revealed that the expected annual energy yield obtained from the hybrid system will be around 92.18GWh, an amount able to cover the 27.85% of the yearly electricity islands need, which was calculated to be 348.64GWh. The electricity produced from the Photovoltaic units will reach the amount of 20.43GWh, whereas the turbines will contribute significantly more generating around 71.75GWh of electricity. Summer is considered as the most energy productive season due to increased irradiation and wind speed level, leading to an electricity output of 32.93GWh, which constitutes the 36% of the total annual electricity production.

The goal of this study is to prove that renewables can play a key role in the electricity needs of the non-grid connected islands, reducing their fossil fuel dependency and promoting sustainability.



## Contents

Disclaimer.....	3
Acknowledgements.....	3
Abstract.....	3
Contents.....	4
List of figures.....	5
List of tables .....	6
1. Introduction .....	7
1.1. Greek islands and fossil fuel dependency .....	7
1.2 Renewables background .....	7
1.2. Case study and problem's description .....	9
1.3. Geographical data .....	9
1.3.1. Cos.....	9
1.3.2. Calymnos.....	10
1.3.3. Pserimos islet .....	10
2. Aim .....	11
3. Research Questions.....	12
4. Methodology Steps .....	13
4.1. PV energy yield calculation methodology (equations and assumptions) .....	13
4.2. Wind energy yield calculation methodology (equations and assumption) .....	19
5. Obtained energy from the hybrid system.....	21
6. RESULTS (Electricity consumption of Cos and Calymnos).....	22
7. RESULTS (Photovoltaic part) .....	25
7.1. Horizontal irradiation estimation.....	25
7.2. Favorable PV location identification .....	27
7.3. PV modules .....	30
7.4 Tilted radiation estimation .....	32
7.5. PV panels expected produced energy yield.....	39
7.6. PV system's total efficiency calculation .....	45
8. RESULTS (Wind park part) .....	46
8.1. Wind speed estimation .....	46
8.2. Wind park location identification .....	49



8.2.1. Wake effect .....	50
8.2.2. Wind speed decrease due to Wake's effect .....	52
8.2.3. Hill speed up effect .....	53
8.2.4. Tunnel speed up effect .....	53
8.2.5. Wind turbines sitting spots selection .....	55
8.3. Air density .....	56
8.4. Technical characteristics of the selected wind turbine model Vestas V100-2MW .....	58
8.5. Energy yield produced by the wind system .....	59
9. Total energy produced from the hybrid system .....	63
10. Participation share of the hybrid system in the actual electricity consumption of Cos and Calymnos .....	65
11. Conclusions .....	66
12. Recommendations .....	67
Bibliography .....	68
Appendix A- Sun's declination .....	71

## List of figures

Figure 1: Profits gained per year from off (islands) and on grid installations .....	8
Figure 2: Cos island .....	10
Figure 3: Calymnos island .....	10
Figure 4: Pserimos islet .....	11
Figure 5: Dodecanise complex .....	11
Figure 6: Electricity consumption of Cos and Calymnos for 2013 .....	22
Figure 7: Electricity consumption of Cos and Calymnos for 2014 .....	22
Figure 8: Comparison of 2013 and 2014 electricity demand.....	23
Figure 9: SoDa software .....	25
Figure 10: Global horizontal-Diffuse horizontal-Reflected horizontal irradiation .....	26
Figure 11: Total monthly direct beam irradiation.....	27
Figure 12: PV instalation location .....	28
Figure 13: Declination angle ( $\delta$ ) .....	29
Figure 14: Sunovation panel characteristics .....	30
Figure 15: Total monthly Diffuse and Reflected tilted irradiation .....	33
Figure 16: Sun angle ( $\beta$ ) during 1st of January.....	36
Figure 17: Sun's azimuth ( $\phi_s$ ) fluctuation during 1st of January and July .....	36
Figure 18: $\cos(\theta)$ fluctuation during winter and summer days.....	37
Figure 19: $R_b$ fluctuation during summer and winter .....	38
Figure 20: Tilted beam radiation for Sout-East orientation.....	38



Figure 21: Monthly total tilted radiation in kWh/m <sup>2</sup> .....	39
Figure 22: Kt montly fluctuation .....	40
Figure 23: Average monthly panels efficiency( np) fluctuation.....	43
Figure 24: Energy produced with and without miscellaneous and power conditioning losses .....	44
Figure 25: Wind speed measurement data at reference height (10m) .....	46
Figure 26: Wind speed data at hub height (95m). .....	47
Figure 27: The monthly frequency of wind's direction.....	48
Figure 28: Pserimos.....	49
Figure 29: Wake effect.....	50
Figure 30: Proper wind turbines placing.....	51
Figure 31: Wins flow when passing over a hill.....	53
Figure 32: Wind turbine takes advantage of tunnel effect.....	54
Figure 33: Wind turbines location .....	55
Figure 34: Air's density fluctuation at hub height.....	57
Figure 35: Power curve of Vestas V100-2.0 MW model.....	59
Figure 36: Expected energy produced from wind turbines (1-15).....	60
Figure 37: Expected energy produced from each wind turbine (16-19) .....	61
Figure 38: Expected energy produced from wind turbines 20-21.....	62
Figure 39: Total energy production from the wind system .....	62
Figure 40: Productivity share of each month.....	63
Figure 41: Produced energy yield by the hybrid system.....	64
Figure 42: Comparison of the actual electricity demand of Cos and Calymnos with the electricity produced by the hybrid system .....	65

## List of tables

Table 1: Progress of renewables in Greece (2007-2014).....	7
Table2: Average electricity consumption per season in GWh.....	24
Table3: Average monthly declination and tilt angle.....	29
Table 4: Hourly sun angle ( $\omega$ ) .....	35
Table 5: Sun height angle ( $b$ ) .....	35
Table 6: Mean monthly daylight temperature .....	41
Table 7: Panels temperature ( $T_c$ ) and correction's factor ( $C_f$ ) monthly fluctuation .....	42
Table 8: Miscellaneous and power conditioning losses of the PV modules .....	44
Table 9: The monthly efficiency of the PV system.....	45
Table10: The frequency of wind blowing direction in Pserimos.....	48
Table 11: Stable factors of air's density .....	56
Table12: Technical characteristics of Vestas V100-2MW model.....	58
Table 13: Declination per day .....	71



## 1. Introduction

### 1.1. Greek islands and fossil fuel dependency

The islands are the main characteristic of Greece's morphology and an integral part of the country's culture and tradition. Greek sovereign land includes 6,000 islands and islets scattered in the Aegean and Ionian Seas, of which only 227 islands are inhabited. This is a truly unique phenomenon for the European continent (Greek tourist organisation, 2014).

Due to the fact that the islands are usually located away from the mainland, most of the times tend to be isolated, therefore there is a need of self-dependency as far as water supply, petroleum import and electricity production is considered. The majority of them are facing high electricity production problems due to increased consumption needs, especially during the summer months, when the touristic period starts (Tsakiris, 2010). Most of the islands are electrically self-supplied with the operation of individual fossil fueled power plants. The alternative would be a connection with the main land's grid, which is only possible with the use of submarine cables. However this process most of the times is considered as financially inefficient due to enormous distances in-between the two spots, leading to increased installation and maintenance costs (Terabit, 2014).

Another question that is raised and needs to be answered is why so much focus has been given to fossil fuel dependency, when the geographical location of Greek islands offers a variety of alternatives based on green energy development. In particular, the wind and solar dynamic potentials are quite attractive for PV and wind turbine installations (Mihalakou, 2002). At this moment, the renewables in islands reach in the best case scenario only 20% of the total produced energy (econews.gr, 2015), making them highly dependent from petroleum import. The lack of subsidies and appropriate legislation coupled with the fear of losing the image of the "absolute vacation destination" keep renewables establishment decreased.

### 1.2 Renewables background

Renewables development in Greece started increasing with a progressive rhythm during the last decade. According to the progress report of 2014, the total installed power of electricity production units from renewables was growing steadily the last years with an average increase rate of 25% yearly (ICAP, 2014). For the PV installations and the wind parks the growth during these years is immeasurable taking into consideration that for 2009 the total capacity of PV and wind was 9MW and 846MW respectively and in the end of 2011 it reached the amount of 1500W and 4000MW.

Installed power from renewables in MW (2007-2014)						
Year	Hvdro	Wind parks	PV	Biomass	Total	Increase
2007	95	846	9	39	989	15,7%
2008	158	1022	12	40	1.232	24,6%
2009	180	1.140	37	41	1.398	13,5%
2010	197	1.298	191	41	1.727	23,5%
2011	206	1.640	522	45	2.412	39,7%
2014	300	4.000	1.500	200	6.000	248%
*2020	350	7.500	2.200	350	10.400	-

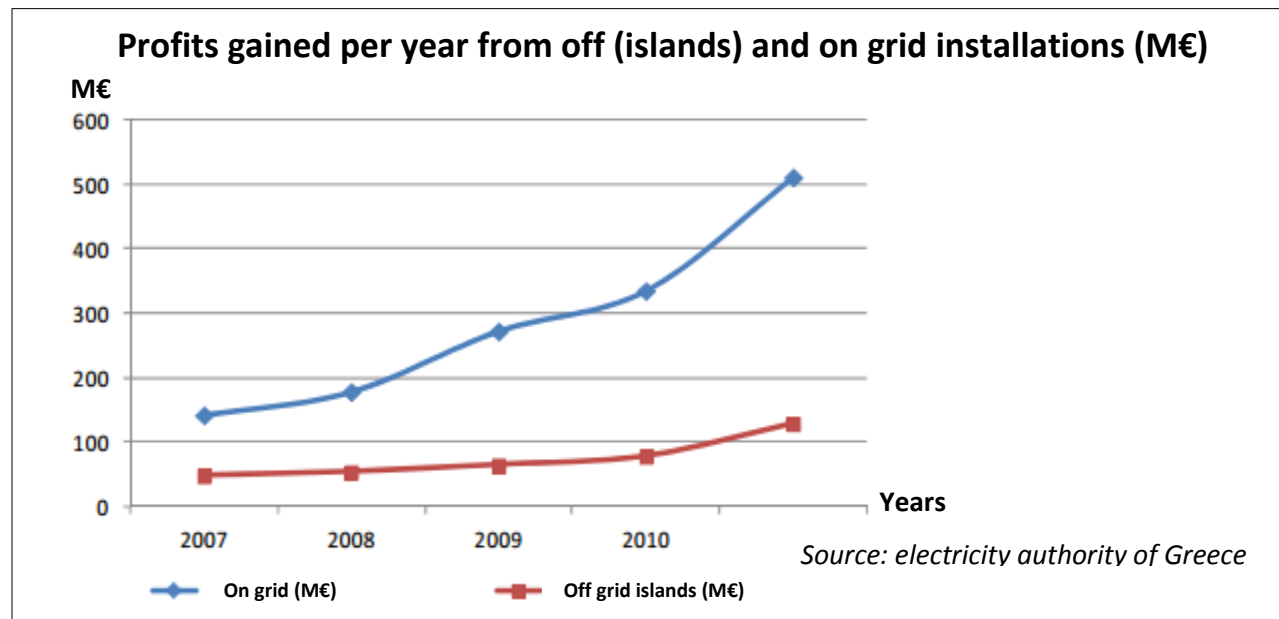
Source: electricity authority of Greece

Table 1: Progress of renewables in Greece (2007-2014)



On table 1 the development of all renewable projects in Greece is depicted, revealing the average increase percentage per year as well as the capacity target of 2020. According to the table the highest investment interest seems to belong in wind turbine installations, since on 2014 the capacity reached the size of 4000MW, almost 3 times higher than PV installations. Hydro and biomass conceive the smallest share concentrating together a total capacity of 500MW. The target for 2020 is to reach the goal of 10400MW, however this is probably an excessively optimistic scenario since the economic crisis has led to a reduction of subsidies as far as renewables investments is considered and to a vertical decrease of energy's price (ICAP, 2014).

In this point it should be clarified that even if the increase of renewables was substantial the last 10 years, around 80% of the total share belongs to on grid installations. The development rhythm as far as off grid projects is considered such as the majority of the Greek islands is much slower (ICAP, 2014). On the next graph (Figure 1) a comparison will take place between the profits gained from off grid (islands) and on grid installations.



**Figure 1: Profits gained per year from off (islands) and on grid installations**

On figure 1 the graphs of yearly profits gained from renewables are depicted. The red line represents the amount of money earned per year from off grid installations that took place in remote islands that were distanced from the main land's grid connection. On the other hand, the blue line represents the yearly profits gained from on grid installations. Analyzing both graphs fluctuation it is noticed that the renewables capacity of on grid installations increased significantly as the years passed by followed by a parallel profits growth. In 2007 the profits were less than 150M€, whereas by the end of 2011 the raise reached the level of 225% resulting in profits of 500 M€. In contrast, the off grid installations presented a small steady profit increase between 2007-2011, however it cannot be compared with the growth of on grid ones. During 2007 the profits were around 50M€ and by the end of 2011 they just passed 100M€, revealing a growth of 110%.





## 1.2. Case study and problem's description

The research subject of this thesis will be the energy investigation of two non-grid connected Greek islands (Cos and Calymnos) and one islet (Pserimos) which belong to the Dodecanese complex located on the south part of the Aegean Sea. Due to the fact that, the overwhelming majority of Greek islands is oil dependent as far as electricity's generation is considered, the need of replacing oil with clean green energy starts becoming an essential issue. Cos and Calymnos are the perfect examples of oil dependent islands where renewables are still in an infant level, covering only 4% of the total consumption need (Giannikos, 2015). The main reason for that neglecting the financial parameters is the negative attitude of the locals against renewables, which is cultivated under the fear of losing the "touristic destination" label.

Cos and Calymnos are 2 highly touristic regions, where especially during the summer suffer from high electricity demand, due to increased fluency of people. For the covering of the electricity needs, two fossil fuel based power plants operate in Cos, providing energy to the local grid, which is also connected with Calymnos (Giannikos, 2015).

In this study focus will be given on the feasibility of fossil fuels reduction or even extinction by installing a PV-Wind hybrid system in the neighboring Pserimos islet, located around 6 miles away from both islands. The installation will be connected with the regional grid via submarine cables and its participation share in the electricity needs of Cos and Calymnos will be examined. The purpose of this research is the utilization of the thousands uninhabited Greek islands as green energy sources targeting towards to sustainability.

## 1.3. Geographical data

In the following section a quick description of the Dodecanese complex as well as Cos, Calymnos and Pserimos will take place, revealing significant geographical and population data according to the latest studies.

### 1.3.1. Cos

Kos or Cos (Figure 2) is a Greek island of the group of the Dodecanese, next to the Gulf of Gökova/Cos. The island measures 40 by 8 km ( $290.300 km^2$ ), and is located 4 km from the coast of Bodrum, Turkey, and the ancient region of Caria (cos.gr, 2015). The island constitutes a municipality within the Cos regional unit, which is part of the South Aegean region. Cos is the third biggest island of Dodecanese right after Rhodes and Karpathos and the second most populated numbering 34.280 citizens according to 2011's inventory.



Figure 2: Cos island

Source: [http://dominicus.malleotus.free.fr/rhodes/lang\\_el/ile\\_kos.htm](http://dominicus.malleotus.free.fr/rhodes/lang_el/ile_kos.htm)

### 1.3.2. Calymnos

On the other hand Calymnos (Figure 3) is located on the southeastern Aegean Sea. It belongs to the Dodecanese complex and its positioned to the west of the peninsula of Bodrum (the ancient Halicarnassos), between the islands of Cos (south, at a distance of 12 km and Leros (north, at a distance of less than 2 km). Calymnos has a population of 16.179, making it the third most populous island of the Dodecanese, after Kos and Rhodes with a land area of  $110.581 \text{ km}^2$  (calymnos.gr, 2015).

The soil of the island is relatively mountainous with small rocky plains and the mountains are treeless with major peaks Prophet Elias, right in the center of the island (760 m.), Kyra High or Karapsili (700 m.) to the South East. and "Galatiani" North West. The coast of Calymnos is relatively steep forming many capes, bays and ports (calymnos.gr, 2015).

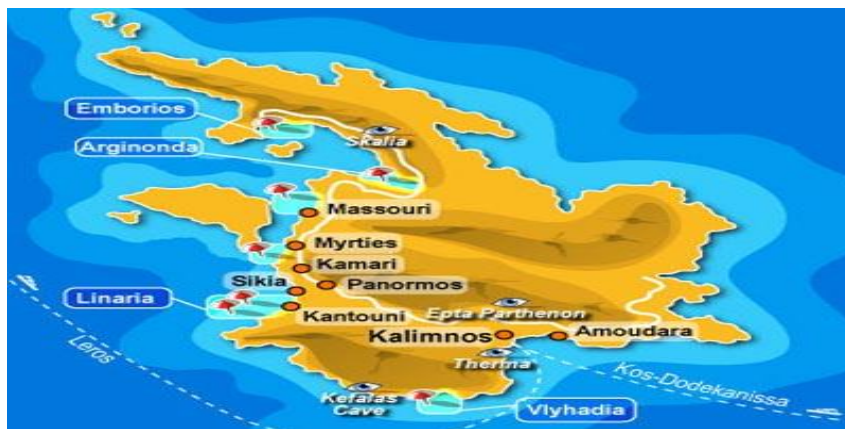


Figure 3: Calymnos island

Source: <http://www.bluetravelgreece.com/kalymnos-island/>

### 1.3.3. Pserimos islet

Pserimos (Figure 4) is a Greek remote island positioned in the southern Aegean sea, which belongs to the Dodecanese complex, with 80 inhabitants based on 2011 inventory. It is located north of Cos and southeast of Calymnos and the surface of the island is around  $14.6 \text{ km}^2$  with a maximum altitude of 268m. Administratively Pserimos consists a part of Calymnos municipality.



Figure 4: Pserimos islet

Source: <http://tsoumpasphotogallery.ning.com/>

On figure 5 the complete map of the Dodecanese complex is presented. All the islands and islets of the complex are dark green colored and it is obvious that they are located near to the South East Greek-Turkish borders. Dodecanese are consisted of twelve main islands and 150 smaller islands and islets, where 26 of them are inhabited. Inside the red cycle Cos, Calymnos and Pserimos islands are highlighted. Additionally, neighbor island groups are depicted on the map such as Cyclades and North East Aegean complex as well as Crete to the South.



Figure 5: Dodecanise comple Source: <http://www.worldatlas.com/webimage/countrys/europe/grdodecanese.htm>

## 2. Aim

The aim of this Thesis is the wind and solar data analysis of Pserimos islet as a favorable PV and Wind turbines installation area for the covering of Cos and Calymnos electricity consumption needs. It will be also assessed the potential electricity production of the installed hybrid system in comparison with the electricity needs per period. The research will be focused only in the energy production part, neglecting the economic aspects.



### 3. Research Questions

The main question of the current study is the following:

**Main question:** *Which will be the expected energy yield of the hybrid system in Pserimos and which will be its contribution share in Cos and Calymnos electricity needs.*

However, for the proper analysis of the topic and the better understanding of the reader, the main question will be split into 5 sub-questions:

- 1 • *Which is the electricity demand of Cos and Calymnos*
- 2 • *What is the annual expected solar energy obtained from the PV park*
- 3 • *What is the annual expected wind energy obtained from the wind park*
- 4 • *What is the total produced electricity of the hybrid's system*
- 5 • *Which will be the contribution of Pserimos hybrid system in Cos and Calymnos electricity needs*

## 4. Methodology Steps

Firstly, the electricity consumption of both islands will be assessed according to hourly data of 2013 and 2014, obtained from the electricity authorities of Cos, since the local grid is interconnected and common (Kyritsis, 2015). Furthermore, the hourly average values will be estimated for a whole year, identifying the months with increased electricity demand.

Thereafter, the energy produced from the hybrid system will be calculated in an hourly, weekly and monthly base revealing the participation share of the total energy needs per period and an in depth analysis will take place. For the prediction of the total expected energy yield produced by the hybrid system installation, the study must split into 2 sub-studies.

- **1) Study focused on the energy yield produced by PV installation**
- **2) Study focused on the energy yield produced by Wind turbines**

Moreover, a comparison between both technologies contribution will take place, based on the individual produced electricity quantity. Last but not least, it will be examined, which will be the share of the total electricity production generated by the hybrid system compared to the actual needs of the islands.

### 4.1. PV energy yield calculation methodology (equations and assumptions)

For the calculation of the Photovoltaic produced energy yield a range of parameters and assumptions must be taken into consideration.

It will be assumed that:

1. The installed PV panels will be mono-crystalline silicon ones with the following characteristics (Sunovation, 2015):

- **Panels efficiency**

- Ambient temperature efficiency → 19.4%
- Temperature loss coefficient (%/°C) → 0.42%/°C

- **Panels Losses**

- 1) Temperature losses → 8%
- 2) Shadings 0 % to 40% (depends of site) → 0%
- 3) Losses weak irradiation → 5%
- 4) Losses due to dust, snow → 2%
- 5) Module array mismatch losses → 2%
- 6) Mismatch efficiency losses → 2,5%

2. The inverter that will be used for the PV installation will be a 20KW, SMA SUNNY TRIPOWER 20000 TL (SMA-hellas.com, 2015):

- Inverter efficiency → 98.5%

- 1) Max DC power → 20440W
  - 2) Max input voltage → 1000V
  - 3) Maximum Power Point voltage range → 320V to 800V/600V
  - 4) Minimum input voltage → 150V
  - 5) Max input current → 33A
3. Shadowing level will be neglected.
  4. The panels will be placed with south orientation due to increased irradiation level (Nuria Novas Castellano, 2015).

Due to the fact, that the analysis will be realistically representative, the PV installation will be placed in the most flat location of Pserimos, targeting to avoid mountains shadowing and inaccessible asymmetrically tilted grounds.

- The methodology steps that will be followed for the calculation of the total energy yield and the efficiency of the PV arrays are presented and analyzed below.

**1<sup>st</sup> step:** Firstly all the components of solar radiation that enter earth's atmosphere must be determined.

1. Diffuse horizontal sky irradiation
  2. Reflected ground irradiation
  3. Direct beam irradiation
- **Diffuse horizontal sky irradiation (H<sub>d</sub>)** is solar irradiation that reaches Earth's surface after having been scattered from the direct solar beam by molecules or suspensoids in the atmosphere (CANMET, 2001-2004).
  - **Solar beam irradiation (H<sub>b</sub>) or Direct Normal Irradiation (DNI)** represents the quantity of sunlight, which passes through the atmosphere, whereas a part of it hits the surface of the Earth in a direct and undisturbed formation. (CANMET, 2001-2004)
  - **Ground reflected irradiation (H<sub>r</sub>)** represents the quantity of solar irradiation that enters into the atmosphere but it is reflected back by the ground (CANMET, 2001-2004).

The sum of these 3 components consists the **Global Horizontal Irradiance (GHI) or H**, which is the total amount of shortwave irradiation received from the atmosphere by a surface horizontal to the ground. Their values will be obtained by satellite data according to the project's location in an hourly base during a whole year (soda-is.com, 2005).

**2<sup>nd</sup> step:** The irradiation that is absorbed by the tilted panels will be broken down into 3 different kinds of absorption and it will be determined using the stated following equations (Shahnawaz Farhan Khahro, 2014).

1. **Diffuse tilted irradiation (R<sub>dt</sub>)** can be calculated using equation 1.

$$1.Hdt = Hd * Rd$$



Where  $R_d$  according to Liu and Jordan isotropic model (Shahnawaz Farhan Khahro, 2014) equals with:

$$2. R_d = \frac{1 + \cos\beta}{2}$$

Where,

- $\beta$  represents the slope of the PV array

Due to the fact that the PV modules will be fixed, the most efficient slope ( $\beta$ ) needs to be determined. In order to do that equation 3 will be implemented for all the days of the year and the resulted average value will be used as the fixed tilt angle of the modules.

$$3. S_m = \Phi - \delta$$

Where,

- $\Phi$  represents location's latitude and equals with  $36.932^\circ$
- $\delta$  represents sun's declination

2. **Reflected tilted irradiation** ( $R_{rt}$ ) can be calculated with the implementation of equation 4.

$$4. H_{rt} = \rho H R_r$$

Where,

- $\rho$  represents the ground albedo of the location
- $H$  represents the GHI of the location
- $R_r$  represents a conversion factor

$$5. R_r = \frac{1 - \cos\beta}{2}$$

3. **Beam tilted or direct normal tilted irradiation** ( $B_{rt}$ ), can be calculated using equation 6

$$6. H_{bt} = R_b * H_b$$

Where,

- $H_b$  equals with:

$$7. H_b = H - H_d$$

- $R_b$  represents a conversion factor, that can be determined using equation 8 (Katsaprakakis, Sun Geometry, 2007)



$$8. Rb = \frac{\cos\theta}{\cos\theta_z}$$

Where,

- $\theta$  represents the incidence angle of beam irradiation per hour of the day
- $\theta_z$  represents the zenith angle of the sun per hour of the day

**3<sup>rd</sup> step:** In order to calculate the Beam Tilted irradiation in an hourly base, the following parameters must be estimated as well.

1: Firstly, the declination  $\delta$ , which is the angular position of the sun at solar noon must be calculated using Cooper's equation (CANMET, 2001-2004).

$$9. \delta = 23.45 \sin\left(2\pi \frac{284+n}{365}\right)$$

Where,

- $n$  represents the day of the year.

2: After the calculation of  $\delta$  for all the days of the year then it's a necessity to calculate the hourly angle of the sun  $\omega$  using the following equation 10 (Katsaprakakis, Sun Geometry, 2007).

$$10. \omega = (t_{sol}-12) \cdot 15^\circ$$

Where,

- $t_{sol}$  represents the time in 24 hour basis

3: The azimuth of the sun ( $\phi_s$ ) in an hourly base is the next parameter that needs to be estimated (Katsaprakakis, Sun Geometry, 2007).

$$11. \sin\phi_s = \frac{\cos\delta \cdot \sin\omega}{\cos b}$$

Where,

- $b$  represents the angle of the sun height at a specific time

4. Sun height  $b$  will be calculated using equation 12 (Katsaprakakis, Sun Geometry, 2007).

$$12. \sin(b) = \cos(\lambda) * \cos(\delta) * \cos(\omega) + \sin(\lambda) * \sin(\delta)$$

Where,

- $\lambda$  is the latitude of the project's location

5: Additionally, the surface's azimuth ( $\phi_p$ ) must be estimated as well. It differs according to the orientation of the surface, however it is known that the orientation of the panels will be south.

6: Zenith angle of the sun  $\theta_z$  will be calculated using equation 13 (Katsaprakakis, Sun Geometry, 2007).

$$13. \theta_z = 90 - b$$

7. The final parameter that needs to be estimated is the incident angle of beam irradiation ( $\theta$ ), which equals with (Katsaprakakis, Sun Geometry, 2007):

$$14. \cos\theta = \cos(b) * \sin(\beta) * \cos(\gamma) + \sin(b) * \cos(\beta)$$

Where,

- $15. \gamma = \phi_s - \phi_p$

**4<sup>th</sup> step:** After completing all the above steps, it will be possible to calculate the hourly irradiation on the plane of PV array  $H\tau$  (A.A. El-Sebaili, 2009).

$$16. H\tau = H_b R_b + R_d H_d + H_p R_r$$

**5<sup>th</sup> step :** The average efficiency  $np$  of the array, which is a function of the average module's temperature ( $T_c$ ), the reference temperature ( $T_r$ ), the panels theoretical efficiency ( $nr$ ) and the temperature coefficient ( $\beta_p$ ) equals with (CANMET, 2001-2004):

$$17. np = nr[1 - \beta_p(T_c - T_r)]$$

Where,

- $T_r$  represents the reference temperature (25°C)
- $\beta_p$  represents the temperature coefficient for module efficiency (%/°C)
- $T_c$  is related to the average monthly ambient temperature  $T_a$  (Evans, 1981)

$$18. T_c - T_a = (219 + 832\overline{K\tau}) \frac{NOCT - 20}{800}$$

Where,

- NOCT represents the Nominal Operating Cell Temperature
- $\overline{K\tau}$  represents the monthly clearness index



Before reaching the surface of the earth, irradiation from the sun is attenuated by the atmosphere and the clouds. The ratio between solar irradiation at the surface of the earth and extraterrestrial irradiation is called clearness index  $\overline{K\tau}$  (Ravinder Kumar, 2005). Thus the daily average clearness index will be:

$$19. \overline{K\tau} = \frac{\overline{H}}{H_0}$$

Where,

- $H_0$  is the daily extraterrestrial irradiation.

However, because the PV arrays tilt angle will not be optimal, the right side of equation 18 must be multiplied with the correction factor Cf (CANMET, 2001-2004).

$$20. Cf = 1 - 1.17 \times 10^{-4} (S_M - S)^2$$

Where,

- $S_M$ : represents the optimum tilt angle
- $S$ : represents the actual tilt angle

**6<sup>th</sup> step:** Thereafter, the energy delivered by the PV array  $E_p$  will be estimated (CANMET, 2001-2004).

$$21. E_p = Snp\overline{H\tau}$$

Where,

- $S$ : represents the area of PV array in  $m^2$
- $\overline{H\tau}$ : represents the monthly average daily irradiance in the plane of the PV array
- $np$ : the average efficiency of the array

**7<sup>th</sup> step:** Finally, the produced PV array energy  $E_A$  that is available can be calculated, taking into account the intermediate losses (CANMET, 2001-2004).

$$22. E_A = E_p(1 - \lambda_p)(1 - \lambda_c)$$

Where,

- $\lambda_p$  represents the miscellaneous PV array losses
- $\lambda_c$  represents other power conditioning losses

**8<sup>th</sup> step:** The overall array efficiency can be calculated using equation 23 (CANMET, 2001-2004).

$$23. n_A = \frac{E_A}{S(\overline{H\tau})}$$



## 4.2. Wind energy yield calculation methodology (equations and assumption)

For the estimation of the potential wind energy yield a range of parameters and assumptions have to be taken into consideration as well.

It will be assumed that:

- **Wind turbine characteristics**

1. The power capacity of each installed wind turbine will be 2MW (average wind turbine power for Europe) (windustry.org, 2014).
2. The wind turbine model will be Vestas V100-2.0MW
3. The hub height will be 95m according to the selected model brochure (Vestas, 2015), when the average hub height for 2014 in Germany is 94m according to statista.com (statista.com, 2015)

Cut in ( $V_{ci}$ ), rated ( $V_r$ ) and cut out ( $V_{co}$ ) wind speed will be equal with 3m/s, 12m/s and 22m/s respectively (Vestas, 2015). The calculation of the wind power production in Watts will be made using equation 24 (Libii, 2013).

$$24. P = \frac{1}{2} * \rho * A * V^3 * C_p * N_g * N_b$$

Where,

- $\rho$  represents the air density in ( $kg/m^3$ )
- $A$  represents the swept area in ( $m^2$ )
- $V$  represents the wind speed in  $m/s$  at hub height
- $C_p$  represents the performance coefficient in(%)
- $N_g$  represents generator's efficiency in (%)
- $N_b$  represents gear box bearing efficiency in (%)

The steps for the estimation of the needed parameters, in order to calculate the produced wind turbines power are presented below:

**1<sup>st</sup> step:** The wind speed data of Pserimos in 10-minute step for the last 2 years will be obtained from the National Observatory of Athens at 10m height (meteo.gr, 2015). Nevertheless, due to the lack of wind-sensors installation in Pserimos, the wind dynamic historical data that will be used were gathered from Kos airport, which is located at a distance of 7 miles away from the research spot.

**2<sup>nd</sup> step:** The obtained wind speed data at 10m height will be integrated for the calculation of the wind speed at 95m hub height, using wind profile power law (Touma, 2012). According to power law relationship the wind speed at 22 height can be estimated using formula 25.

$$25. U_2 = U_1 * (Z_2/Z_1)^a$$

Where,

- U2 represents the wind speed (m/s) at a hub height of 95m
- U1 represents the wind speed (m/s) at the reference measurement of 10m
- Z2 represents the wind speed measurement height of 95m
- Z1 represents the reference wind speed measurement height of 10m
- Exponent  $\alpha$  represents an empirically derived coefficient (unit less), which can be calculated using equation 26 (Katsaprakakis, Wind energy, 2007)

$$26. \alpha = 0.04 * \ln(Zo) + 0.003 * (\ln(Zo))^2 + 0.24$$

Where,

- Zo represents the surface roughness in (m), which equals with 0,032m for Pserimos location (Katsaprakakis, Wind energy, 2007).

**3<sup>rd</sup> step:** Air density is influenced by a variety of factors, from which of them some are stable and some others fluctuate intensively dependent on the weather conditions. Therefore, density will be estimated in a 10 minute step for the whole year (Ioannis Fyrippis, 2010).

$$27. \rho = \rho_o * \frac{T_o}{T} * (1 - \frac{\Gamma - Z}{T_o})^{\frac{g}{\Gamma + R}}$$

Where,

- $\rho_o$  represents the standard air density in sea level and equals with  $1.225 \frac{kg}{m^3}$
- $T_o$  represents the standard temperature at sea level and equals with (288K)
- T represents the environment temperature in (K)
- $\Gamma$  represents the vertical temperature gradient, which will be taken as  $6.5 \frac{K}{km}$
- Z represents the altitude above the sea in (m)
- g represents the gravity acceleration and equals with  $9.81 \frac{m}{s^2}$

**4<sup>th</sup> step:** The swept area will be calculated using equation 28 (Ioannis Fyrippis, 2010).

$$28. A = \pi * R^2$$

Where,

- $\pi$  represents the mathematical constant of 3,14
- R represents the length of the wind turbine's blade in (m)



**5<sup>th</sup> step:** According to the geographical dimensions of Pserimos and the average wind direction, the number of installed turbines will be estimated taking into account the wake effect and the appropriate spacing with each other, in order to avoid the created turbulence and to achieve the best possible performance (F.Gonzalez-Logatt, 2012).

## 5. Obtained energy from the hybrid system

After the calculation of the Photovoltaic and Wind turbines energy yield, the total values will be summed up for the estimation of the total electricity production generated from the hybrid system. The hourly, weekly and monthly expected production will be estimated, however only monthly values will be depicted for space's economy. Furthermore, the total production will be compared with the total electricity consumption that took place in a monthly base during the previous years, revealing the participation share of Pserimos hybrid system.

## 6. RESULTS (Electricity consumption of Cos and Calymnos)

Firstly, the electricity consumption needs of Cos and Calymnos will be presented based on data retrieved from the electricity authorities of Cos for the years of 2013 and 2014 (Kyritsis, 2015).

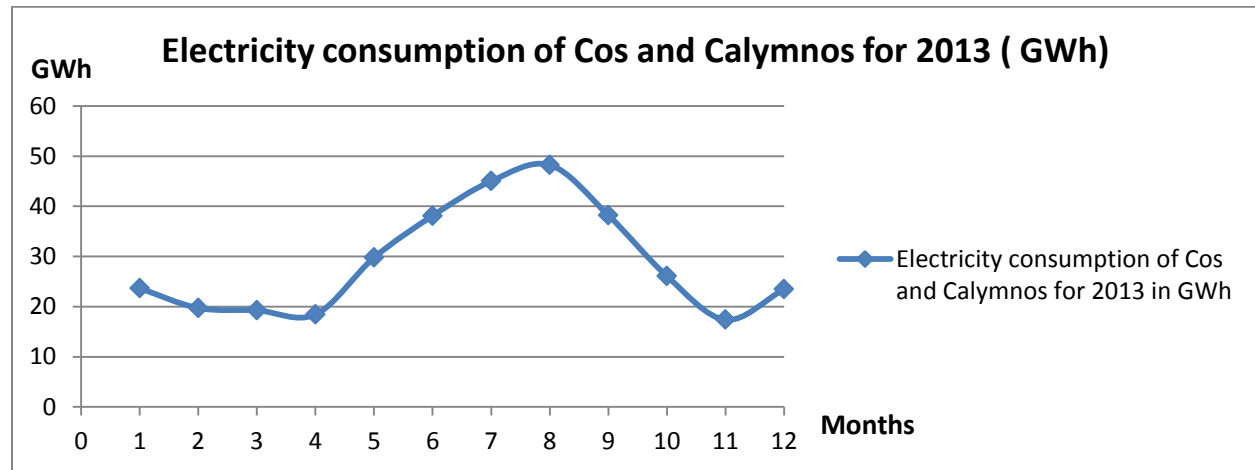


Figure 6: Electricity consumption of Cos and Calymnos for 2013

On figure 6 the electricity consumption of Cos and Calymnos for the year of 2013 is depicted. According to the retrieved data, it is revealed that the monthly consumption fluctuated in-between 18.44GWh and 48.23GWh among the year. Winter's demand was balanced around 20GWh, followed by a slight decrease of 6% during March and April. From May to August a sharp increase of 116.5% took place reaching the highest level of 48.23GWh. Thereafter, an equal decrease dropped down the consumption to the level of 19GWh. The total electricity demand for the whole year of 2013 was 348.75GWh.

This phenomenon can be explained taking into consideration the fact, that specially Cos is a highly touristic island, where during summer period is flooding from people coming to spend their vacation. Additionally, due to high temperature levels during these months, the operation of cooling devices increases dramatically, contributing negatively to the already high electricity consumption.

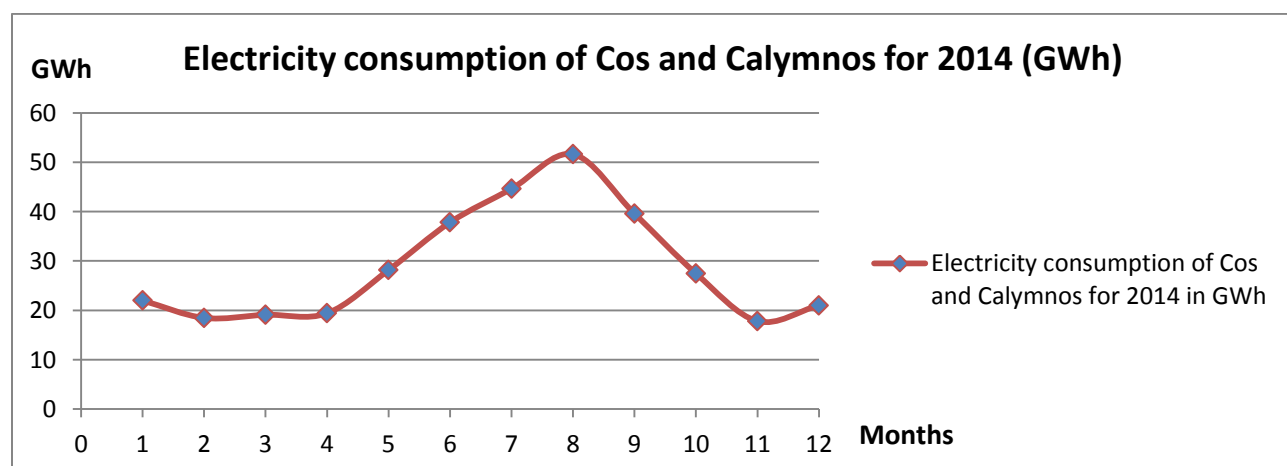


Figure 7: Electricity consumption of Cos and Calymnos for 2014





As far as year 2014 is considered, the consumption fluctuation remained on the same levels with the previous year. Analyzing the graph (Figure 7) it is noticed, that again the consumption need during winter was stable around 20GWh, reaching the peak of 22GWh on January. For one more time, the highest demand month was August overpassing 50GWh. Additionally, spring and autumn periods were characterized as the lowest consumption months, according to the electricity authorities of Cos, leading to monthly values lower than 20 GWh. The total electricity demand for 2014 reached the level of 348.56GWh increased by 0.54% compared with 2013.

Both graphs are similarly shaped with almost unnoticed values differentiation. The description of both years revealed the lowest consumption among the intermediate months of spring and autumn. This result is probably based to the fact, that during these months the use of air conditioning and lighting devices is extremely limited. Moreover, the touristic period has not started yet, therefore the fluency of people in the islands is decreased.

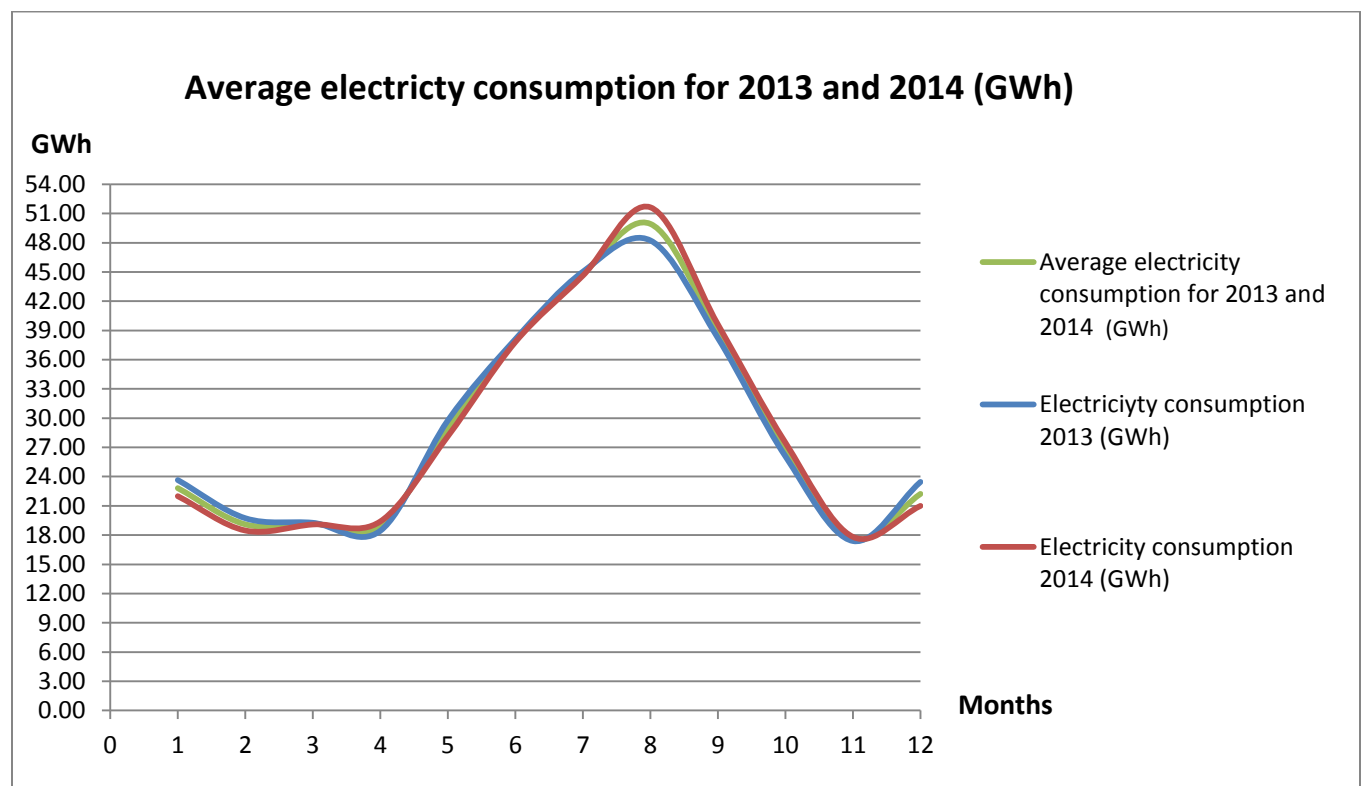


Figure 8: Comparison of 2013 and 2014 electricity demand

On figure 8 the consumption of 2013 and 2014 is depicted with the blue and red color respectively, showing the fluctuation difference of both years. Comparing both graphs, it is concluded that during the winter of 2013 the electricity needs were slightly increased by 8% than the winter of 2014. Furthermore, spring's consumption for 2013 was higher by 1.23%, whereas summer and autumn of 2014 surpassed the previous year by 2% and 3.95% respectively. The green line highlights the average values of the two compared years.

On following table 2 the average season consumption values are analytically presented, verifying the above analysis.

<b>2013-2014 average electricity consumption</b>	
<b>Season</b>	<b>Electricity consumption (GWh)</b>
Winter	21.38
Spring	22.35
Summer	44.24
Autumn	27.76

**Table2: Average electricity consumption per season in GWh**

Observing Table 2 it is noticed that for the study years, the average consumption need during summer is almost doubled in comparison with the rest of the season. Specifically, summer's produced electricity from Cos powerplants is by 100.91%, 97.92%, 59.37% higher than the respective winter's, spring's and autumn's demand.

## 7. RESULTS (Photovoltaic part)

### 7.1. Horizontal irradiation estimation

In the methodology steps, the process that will be followed for the prediction of the total PV energy yield was analytically described.

Firstly, with the use of SODA software (Clive Best, 2005) satellite data of global horizontal, reflected and diffuse horizontal irradiation for the location of Pserimos were obtained. The data were downloaded in an hourly base for a whole year. Due to financial restrictions the average historical irradiation data between the years 2000-2005 were used because the more recent ones are confidential and subscription fee is mandatory.

The data were received according to the location's coordinates (Google Earth, 2015):

- Latitude: 36.932 °
- Longitude: 27.143°


- FREE HChour (2004-2005) - HelioClim3v5 Time-Series of Hourly Solar Irradiance over the Horizontal Plane -

Execute SoDa Service

Enter:  
 1\_ EITHER latitude and longitude (decimal degrees, see [conversion function](#) from degrees, minutes, seconds)  
 2\_ OR search city by name ('search city by name' button)  
 3\_ OR click in the map

1\_ Latitude   
 Longitude

2\_

3\_ 

Enter the altitude (in m). -999 means "use default digital terrain elevation database value".

Select the first date

Select the last date

Enter the ground albedo [0..1]

Take into account the shadows due to relief (slower)?

Output time step: hour

Select the time reference

Output in text file or in screen? (Given the large volume of data that may output from this service, text file is recommended)

Figure 9: SoDa software

On figure 9 the searching software of SoDa is presented. The satellite data can be retrieved by adjusting the date and the proper ground albedo value of the location. Moreover, the coordinates of the studied area must be inserted as well. All the above parameters are highlighted inside the depicted red cycles.

On figure 10 the total monthly received Global horizontal diffuse and reflected irradiation is presented.

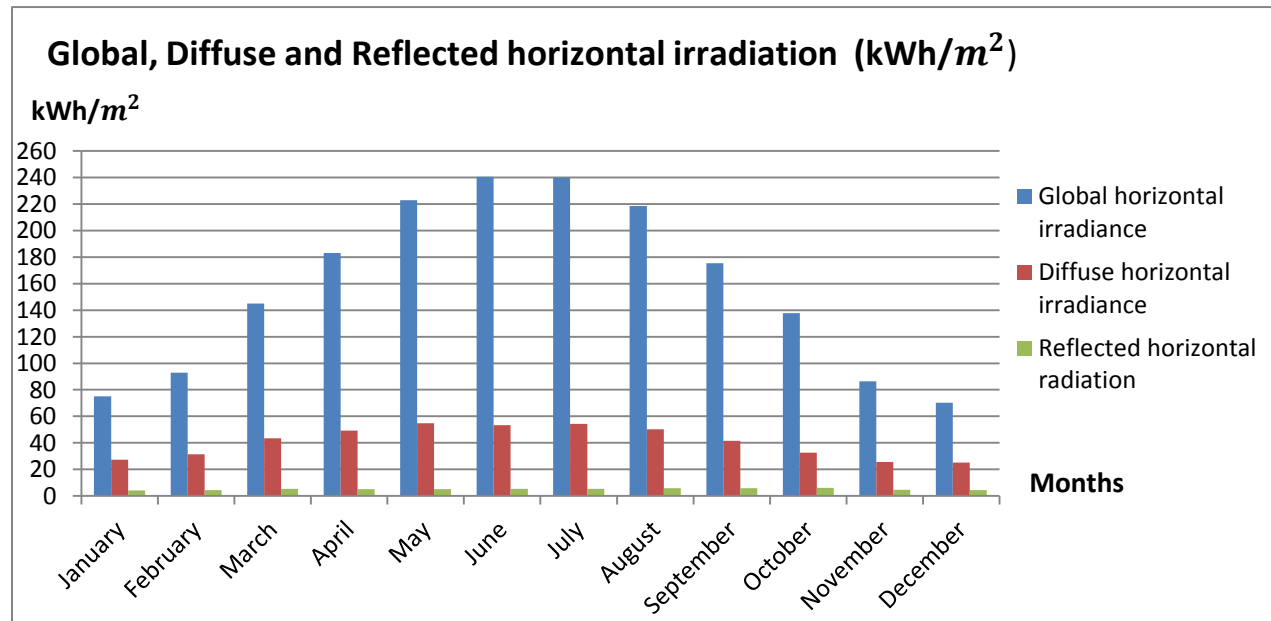


Figure 10: Global horizontal-Diffuse horizontal-Reflected horizontal irradiation

- **Global horizontal irradiation**

The graph (Figure 10) reveals that GHI monthly quantity fluctuates from  $75.24 \text{ kWh/m}^2$  during December to  $240.52 \text{ kWh/m}^2$  on June. Generally, there is a steep irradiation increase after February when the summarized irradiation grows almost vertically reaching  $240.52 \text{ kWh/m}^2$  and  $239.7 \text{ kWh/m}^2$  on June and July respectively. Thereafter, a sudden equally high decrease takes place signifying winter's approach. The yearly average GHI is  $165.30 \text{ kWh/m}^2$  per month and the percentage difference between December (bottom) and July (peak) is 223.78%.

- **Diffuse horizontal irradiation**

According to the graph (Figure 10), the Diffuse horizontal irradiation level varies significantly from  $14.5 \text{ kWh/m}^2$  to  $56.58 \text{ kWh/m}^2$ . The fluctuation is similar with GHI's graph identifying a progressive increase from February and towards reaching the peak of  $56.58 \text{ kWh/m}^2$  on July. Afterwards, diffuse irradiation decreases symmetrically until November, when it drops down to  $14.5 \text{ kWh/m}^2$ . A decrease of 390.56% compared with July. The yearly average Diffuse horizontal irradiation per month is  $41.26 \text{ kWh/m}^2$ .

- **Reflected horizontal irradiation**

As far as reflected irradiation is considered, the differentiation among the year is quite slighter compared with the other categories. The fluctuation varied between  $4.28\text{kWh}/\text{m}^2$  and  $6.10\text{kWh}/\text{m}^2$ . Similarly, the irradiation level increased during the summer, however the peak value of  $6.10\text{kWh}/\text{m}^2$  was achieved on October. The yearly average value was estimated as  $5.173\text{kWh}/\text{m}^2$  and the fluctuation difference from the peak month of October to the bottom month of January reaches the level of 29.86%.

With the above data obtained by SoDa software, the hourly Direct beam irradiation can be calculated. It can be determined by subtracting the Diffuse horizontal from the Global horizontal irradiation using equation 6 (CANMET, 2001-2004). Reflected irradiation is neglected due to the fact that its values are close to zero.

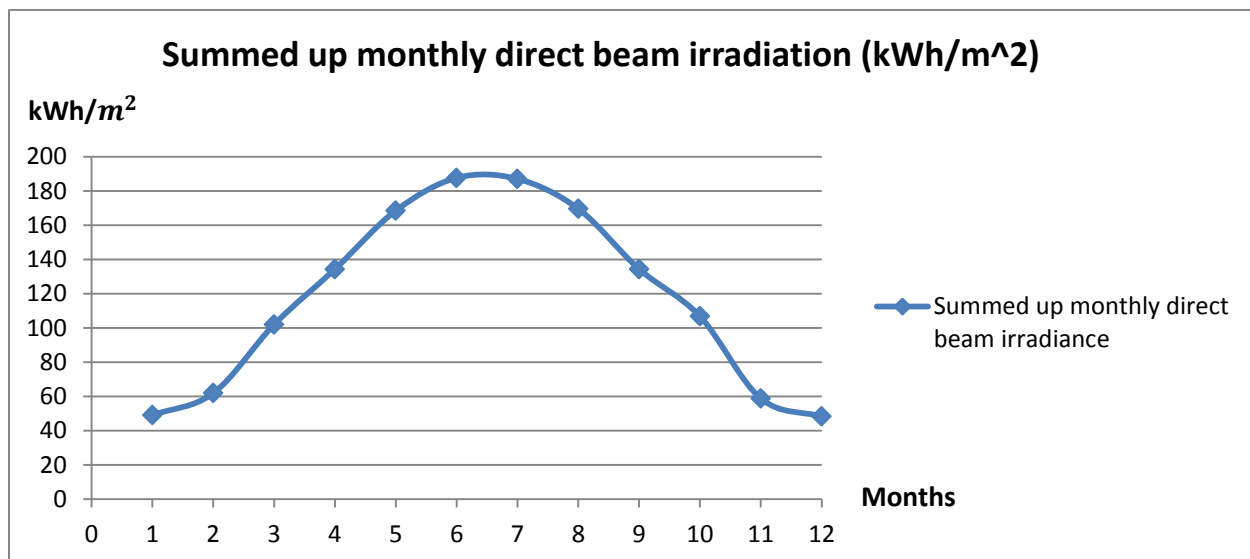


Figure 11: Total monthly direct beam irradiation

The monthly graph of direct beam irradiation (Figure 11) reveals similarities with the previous graphs. In this case, the values increase highly as months pass by reaching the peak of  $187.65\text{kWh}/\text{m}^2$  on July. After August it decreases analogically with the previous increase until December, when it drops down to the lowest levels of  $48.20\text{kWh}/\text{m}^2$ .

## 7.2. Favorable PV location identification

Since all the components of sun's horizontal irradiation are obtained or calculated, the next step is the estimation of the tilted PV irradiation. However, it's a priority need to identify first the most suitable location for the Photovoltaic installation. Due to the fact that, Pserimos is a mountainous region with high surface fluctuations (Google Earth, 2015), it is quite difficult to access and install Photovoltaic units through the paths of the island. Even if that was possible, shadowing from the nearby mountains would affect the efficiency of the modules. Therefore, the most flat surfaces must be identified for the construction of horizontal platforms which will allow the PV installation above them (Papadopoulos, 2015). To achieve that, Google Earth software will be used, revealing the magnitude of the island's surface anomaly.

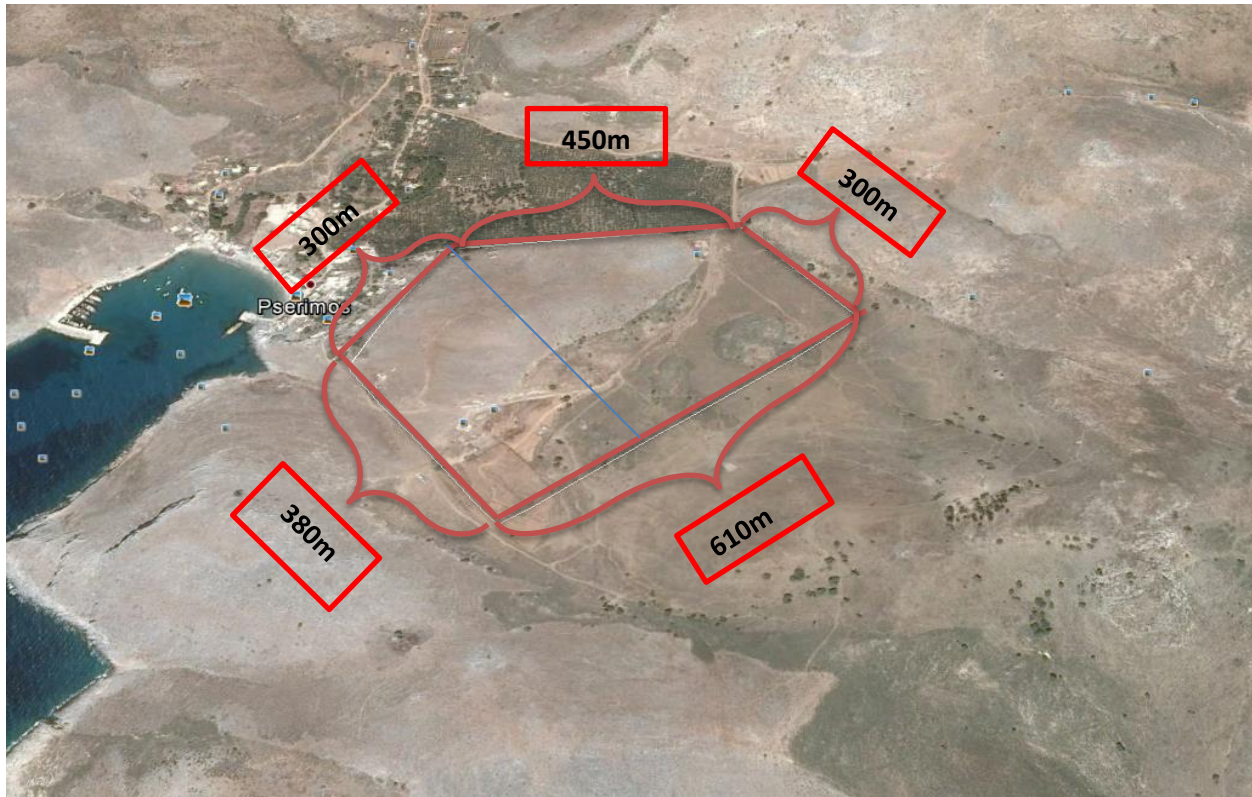


Figure 12: PV instalation location

On figure 12 the most flat location on the south part of Pserimos is depicted. According to the above, surface elevation inside the red cycle varies from 22 to 35m (Google Earth, 2015). The total land area was calculated using the <<add path>> tool of Google Earth software and equals with  $197800m^2$ .

Because the fluctuation is smooth without sudden steep alternations, 4 different platforms every 4m of ground altitude change will be installed making the construction horizontal and parallel to the sea level. Next to the selected red area a cultivation field is located, which is favorable for PV installation due to the righteousness that it has. However, it is forbidden from Greek legislation, since it's considered as agricultural territory (ypeka.gr, 2015).

Moreover, the most efficient tilt angle for the appropriate placing of the panels must be estimated as well. The most optimum angle differentiates per hour of the day, per day and per month. In this case, the best tilt angle per day will be calculated according to equation 3 (Nuria Novas Castellano, 2015) and the monthly average is presented on the following table 3.

$$3. Sm = \Phi - \delta$$

Where,

- $\Phi$  represents the location's latitude and equals with  $36.932^\circ$
- $\delta$  represents sun's declination

In order to calculate  $S_m$ , firstly the daily sun's declination will be estimated according to Cooper's equation 8 (CANMET, 2001-2004).

$$\delta = 23.45 \sin\left(2\pi \frac{284 + n}{365}\right)$$



Figure 13: Declination angle ( $\delta$ )

Declination ( $\delta$ ) remains the same and it's not fluctuating during the day, however the value of  $\delta$  changes per day of the year as it's depicted in Appendix A. According to the obtained results,  $\delta$  value is negative during winter and autumn varying from  $-23.45^\circ$  on 22 of December to  $0^\circ$  on March 11 (Figure 5). From April to June the values are positive and sharply increased reaching  $23.45^\circ$  on June 21. Thereafter, they start decreasing again progressively remaining positive until the 23<sup>rd</sup> of September when  $\delta$  value becomes  $0^\circ$  once more.

On following table 3, the average monthly values of  $\delta$  and  $S_m$  are depicted showing the variation of the monthly mean declination and the most efficient tilt angle per month.

Months	Average monthly $\delta(^{\circ})$	Average monthly $S_m(^{\circ})$
January	-20.85	57.78
February	-13.33	50.26
March	-2.39	39.32
April	9.49	27.44
May	18.81	18.13
June	23.08	13.85
July	21.10	15.83
August	13.30	23.64
September	1.99	34.94
October	-9.85	46.78
November	-19.05	55.98
December	-23.10	60.03
Yearly Average		<b>37.00</b>

Table3: Average monthly declination and tilt angle



- **Declination ( $\delta$ )**

On table 3 the average monthly values of declination are depicted. The averages fluctuate between  $-23.10^\circ$  and  $23.08^\circ$  during December and June respectively. Observing the results, the values are negative during winter and smoothly increase until June reaching the average of  $23.08^\circ$ . Thereafter, a steady decrease takes place until September when it drops down to  $0^\circ$  and becomes negative the following months.

- **Tilt angle (SM)**

During winter season the most efficient average incline of the modules is  $56.02^\circ$ , however as the weather becomes warmer and summer approaches, the favorable tilt angle decreases significantly reaching the average of  $28.30^\circ$  and  $17.70^\circ$  on spring and summer season respectively. Especially, during June the most efficient module angle tends to be horizontal dropping down to  $13.85^\circ$ , whereas the upcoming months the ideal tilt angle increases reaching the highest level of  $60.03^\circ$  on December. Due to the fact that, the panels will not be accompanied with truckers following sun's direction, PV placing angle should be equal with the year's average of  **$37.00^\circ$** .

### 7.3. PV modules

Since the most efficient tilt angle of the modules has been obtained, focus must be given to the PV installation. At this paragraph the number of the installed PV panels will be roughly estimated using the panel characteristics of Sunovation (Sunovation, 2015). The selection of these panels was based on high efficiency criteria since they are mono-crystalline offering more than 19% efficiency.

According to Sunovation.com the framed modules have 1.63m length and 0.986m width. The total panel area is  $1.61m^2$ , whereas the PV cells cover 98.76% of module's construction (Sunovation, 2015). Additionally, the nominal power of each module will be 278W with  $V_{oc}=39.2V$  and  $I_{sc}=9.67A$ .

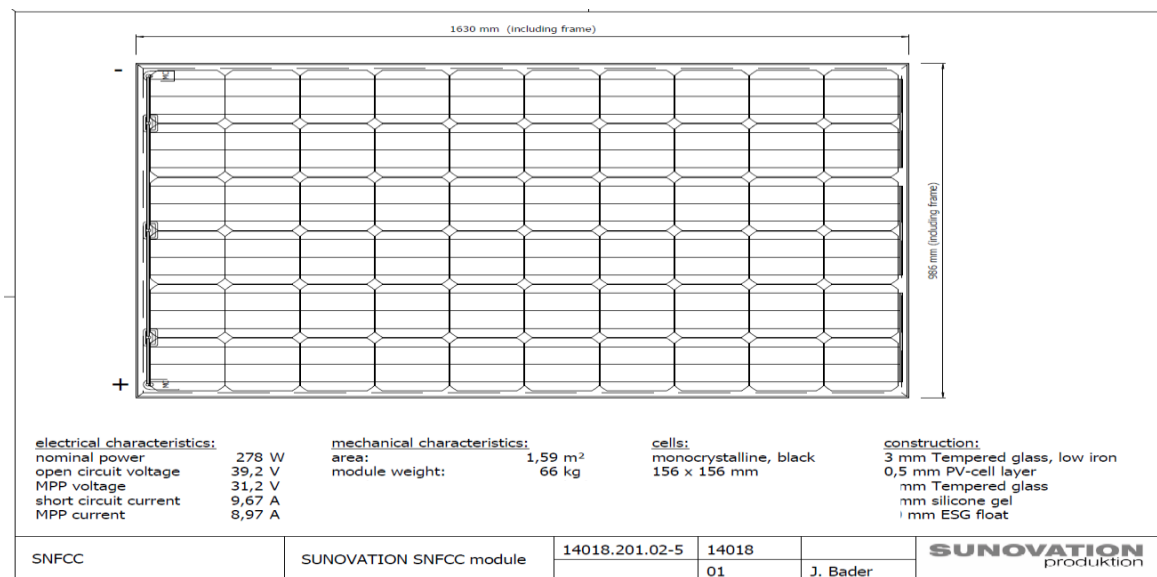


Figure 14: Sunovation panel characteristics

Source: Sunovation.com

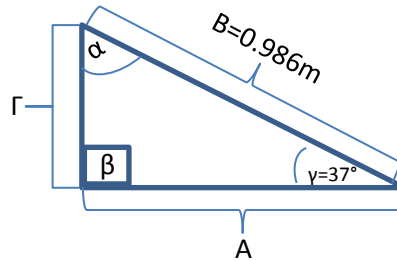
On figure 14 Sunovation panel is depicted. The panel is consisted of 60 mono-crystalline cells covering an area of  $1.59m^2$ . Each cell's dimensions are 156 x 156mm producing a power of 4.63W. However, due to the existence of small gaps inside the panel, the clear PV area is calculated to be  $1.46m^2$ . The panels will be placed in the flattest area of the island, which is located close to the harbor, easy accessible from the local road (Figure 12).

Since the PV area has been estimated, the next step is the examination of how the module arrays will be placed. The first step is the calculation of the minimum distance between the arrays, in order to avoid possible shadings from one panel to the other (Nuria Novas Castellano, 2015). According to Castellano, the distance (d) measured between the horizontal rows of the panels of height must be estimated using equation 29.

$$29. d \leq L * k$$

Where,

- L represents panel's height in (m)
- k represents a unitless parameter, which equals with  $\frac{1}{\tan(61-\varphi)}$
- Height L can be calculated using trigonometry equations. Since the module's installation will create a right triangle with the based platform and the tilt angle together with the one side are known, sinus law can be implemented.
- Tilt angle  $\alpha$  can be estimated using trigonometry equation 30, where the sum of the triangle angles equals with  $180^\circ$ .



$$30. \alpha + \beta + \gamma = 180^\circ$$

Where,

- $\alpha$ ,  $\beta$  and  $\gamma$  represent the angles of the triangle

Since  $\beta$  and  $\gamma$  are known,  $\alpha$  can be estimated and equals with:  $\alpha = 180^\circ - 90^\circ - 37^\circ = 53^\circ$

- Implementing sinus law  $\frac{B}{\sin\beta} = \frac{\Gamma}{\sin\gamma}$ , height  $\Gamma$  will be obtained, equaling with  $\Gamma = \frac{B * \sin\gamma}{\sin\beta} = 0.59m$

According to the obtained dimensions of the tilted module, distance d can be estimated and equals with  **$d \leq 1.33m$**



- Afterwards, for the calculation of minimum distance (D), the obtained distance (d) must be added to the horizontal projection of the panel of length (L) at an angle of inclination ( $\beta$ ) (Nuria Novas Castellano, 2015).

$$31. D = L * \cos\beta + d$$

- According to equation 31 of Castellano, the minimum distance between the modules should be 1.8m.
- Based on the above results the total number of installed PV panels will be calculated by dividing the total used land area with the area covered from one PV panel coupled with the respective distance(D), which equals with:

$$197800m^2 / (0.986 + 1.8)m * (1.63)m = 197800m^2 / 4.54m^2 = 43568 \text{ panels}$$

According to, the obtained number of installed panels, the clear PV area of the whole Photovoltaic park equals with  $43568 * 1.46m^2 = 63610m^2$ .

#### 7.4 Tilted irradiation estimation

Since the best yearly average angle for the panels installation was calculated to be  $37.00^\circ$ , the received irradiation from the PV inclined surface can be estimated. The procedure steps are presented below.

##### STEPS

1. In order to calculate Hdt equation 1 of methodology has been used (CANMET, 2001-2004).

$$1.Hdt = Hd * Rd$$

Where,

- Rd according to Liu and Jordan isotropic model (Shahnawaz Farhan Khahro, 2014) (equation 2) equals with:

$$2.Rd = \frac{1+\cos\beta}{2}$$

2. For the calculation of Hrt equation 4 of methodology was implemented (Shahnawaz Farhan Khahro, 2014).

$$4.Hrt = \rho HRr$$

The obtained total monthly values of the Diffuse tilted (**Hdt**) and Reflected tilted (**Hrt**) irradiation are depicted on Figure 15.

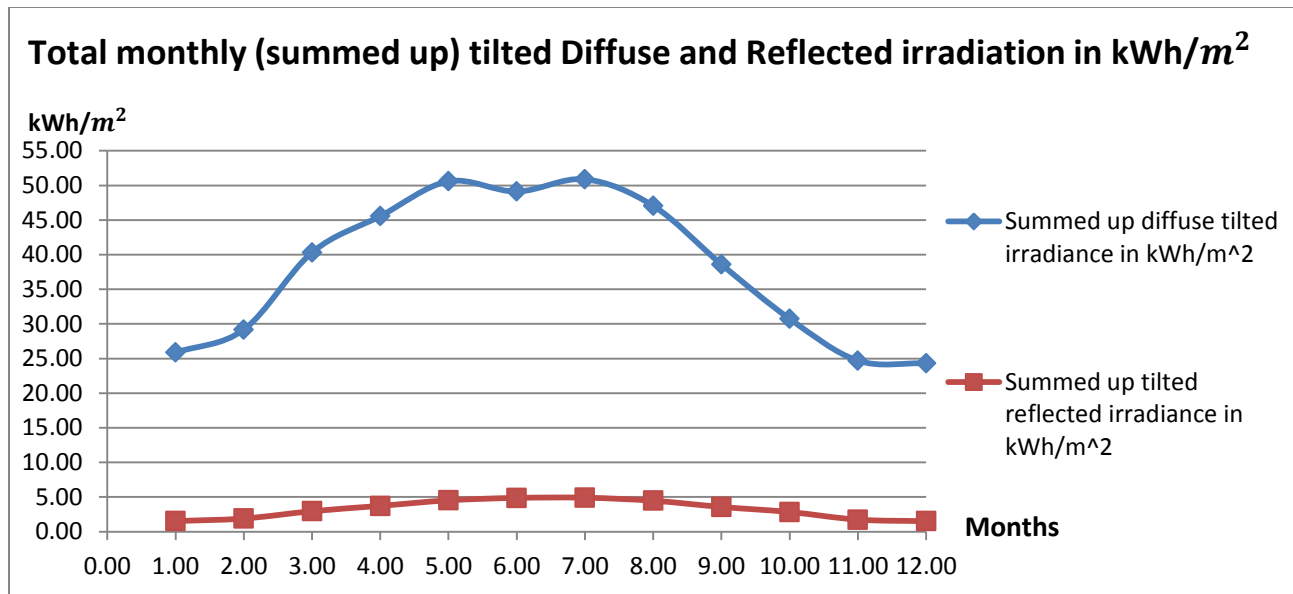


Figure 15: Total monthly Diffuse and Reflected tilted irradiation

- **Diffuse tilted irradiation**

According to figure 15 the Diffuse tilted irradiation through the year fluctuates among 24.32kWh/m<sup>2</sup> and 50.89 kWh/m<sup>2</sup>. During winter months the lowest levels are depicted and vary from around 25 kWh/m<sup>2</sup> on December to 30 kWh/m<sup>2</sup> on February. Afterwards, Diffuse tilted irradiation increases progressively reaching the highest level of 50.89 kWh/m<sup>2</sup> on July. The following months, as winter approaches irradiation decreases with the same rhythm.

- **Reflected tilted irradiation**

As far as Reflected tilted irradiation is considered, the values are considerably lower in comparison with these of Diffuse tilted irradiation and vary between 1.52 kWh/m<sup>2</sup> to 4.91 kWh/m<sup>2</sup>. The graph's fluctuation is similar with the previous case, revealing that again during winter irradiation is significantly lower and increases as months pass by till July.

**3.** For the calculation of hourly Direct beam tilted irradiation (**Hbt**), equation 6 of methodology has been used.

$$6.Hbt = Rb * Hb$$

In order, to calculate Rb a variety of parameters must be taken into consideration. As it is known from equation 8.  $Rb = \frac{\cos\theta}{\cos\theta_z}$ , where  $\theta$  represents the incidence angle and  $\theta_z$  the zenith angle of the sun (Katsaprakakis, Sun Geometry, 2007).

According to Katsaprakakis the incidence angle can be estimated using equation 14.

$$14. \cos\theta = \cos(b) * \sin(\beta) * \cos(\gamma) + \sin(b) * \cos(\beta)$$

- I. Firstly, hourly sun's angle  $\omega$  was calculated using equation 10 of methodology substituting  $tsol$  with all the hours of the day (Katsaprakakis, Sun Geometry, 2007).

$$10. \omega = (tsol - 12) * 15^\circ$$

- II. Thereafter, angle  $b$  was calculated according to methodology's equation 12 of Katsaprakakis (Katsaprakakis, Sun Geometry, 2007).

$$12. \sin(b) = \cos(\lambda) * \cos(\delta) * \cos(\omega) + \sin(\lambda) * \sin(\delta)$$

- III. After the calculation of the above parameters, it was possible to estimate sun's azimuth using equation 10 (Katsaprakakis, Sun Geometry, 2007).

$$10. \sin\phi_s = \frac{\cos\delta * \sin\omega}{\cos b}$$

- IV. Finally, to find  $\gamma$  the surface and sun's azimuth must be estimated using equation 15.

$$15. \gamma = \phi_s - \phi_p$$

The surface azimuth ( $\phi_p$ ) is only influenced by the orientation of the PV panels (Katsaprakakis, 2007). The values that it takes according to modules orientation are the following:

North  $\longrightarrow$   $-180^\circ$

**South  $\longrightarrow$   $0^\circ$**

East  $\longrightarrow$   $-90^\circ$

West  $\longrightarrow$   $90^\circ$

PV panels will be installed tilted to the **South**, as the most efficient orientation according to Greece's coordinates (Nuria Novas Castellano, 2015). Therefore, parameter  $\gamma$  (equation 15) was calculated only for the pronounced case.

All the above parameters were calculated in an hourly basis for a whole year. In the following tables the monthly averages are presented showing the values variation through the year. However, in some cases the hourly values of a random winter and summer day will be presented for better explanation of the parameters fluctuation.



- Hourly sun angle ( $\omega$ )

Time (Hours)	$\Omega(^{\circ})$
1	-165
2	-150
3	-135
4	-120
5	-105
6	-90
7	-75
8	-60
9	-45
10	-30
11	-15
12	0
13	15
14	30
15	45
16	60
17	75
18	90
19	105
20	120
21	135
22	150
23	165
24	180

Table 4: Hourly sun angle ( $\omega$ )

All the hours of the day are used for the calculation of hourly ( $\omega$ ) angle. ( $\omega$ ) will remain the same during the whole year for each specific hour. It takes values from  $-165^{\circ}$  to  $180^{\circ}$  and it varies by  $15^{\circ}$  hourly (Table 4). The time of solar noon is 0.

- Angle of sun height  $b$

Months	$\text{Sin}b(^{\circ})$	$b(^{\circ})$
January	-0.214	-15.600
February	-0.137	-9.927
March	-0.025	-1.679
April	0.099	7.411
May	0.195	14.183
June	0.236	17.194
July	0.216	15.851
August	0.137	10.058
September	0.022	1.599
October	-0.103	-7.410
November	-0.196	-14.378
December	-0.235	-17.097

Table 5: Sun height angle ( $b$ )



The reason why, all the months are close to zero and some of them are negative, is because the night time is included and due to lack of sunlight, these hours (b) is negative. To understand that better, on the following graph a comparison between the sun angle (b) of the 1<sup>st</sup> of January and 1<sup>st</sup> of July as 2 different period days (winter-summer) is depicted.

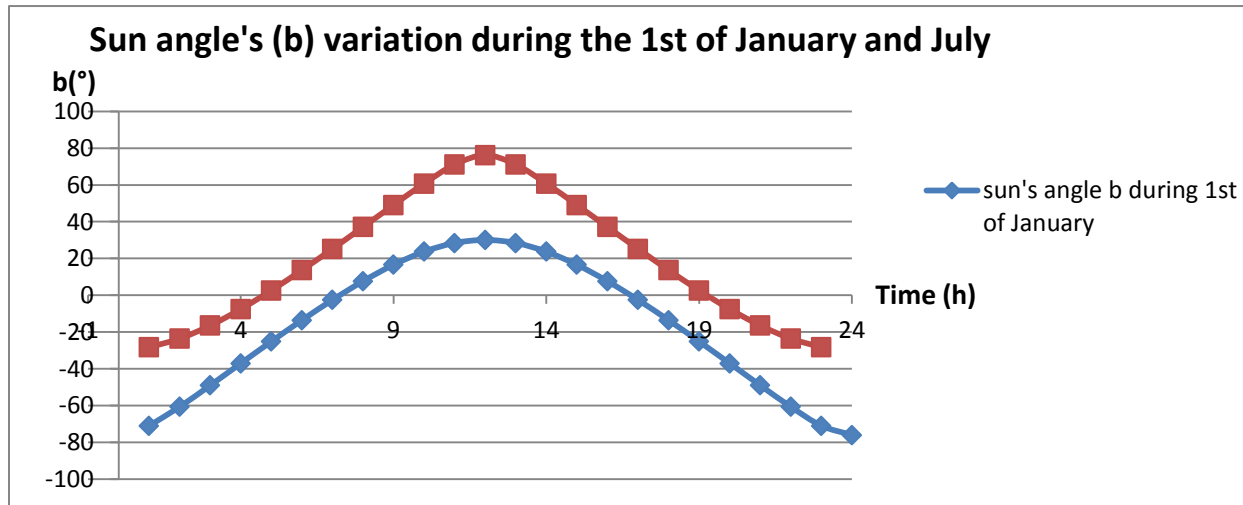


Figure 16: Sun angle (b) during 1st of January

On Figure 16, a comparison of sun's angle b fluctuation between 2 different days of the year is depicted. With the blue line the variation of (b) for the 1<sup>st</sup> of January is presented. During this winter-day it is noticed that, the values of (b) are negative among the night and start increasing as sun rising approaches. Afterwards (b) becomes positive and increases till solar noon. During the rest part of the day (b) starts decreasing again symmetrically until sunset when it becomes 0 again and as the night falls it takes negative values. The same happens also during the 1<sup>st</sup> of July, with the difference that (b) becomes positive faster, due to the fact that sun rising takes place earlier. The peak of (b) at solar noon is over-doubled compared with the winter's graph reaching 80° and the values of sun's angle start becoming negative after 20:00pm when sunset comes.

- Sun's azimuth ( $\phi_s$ )

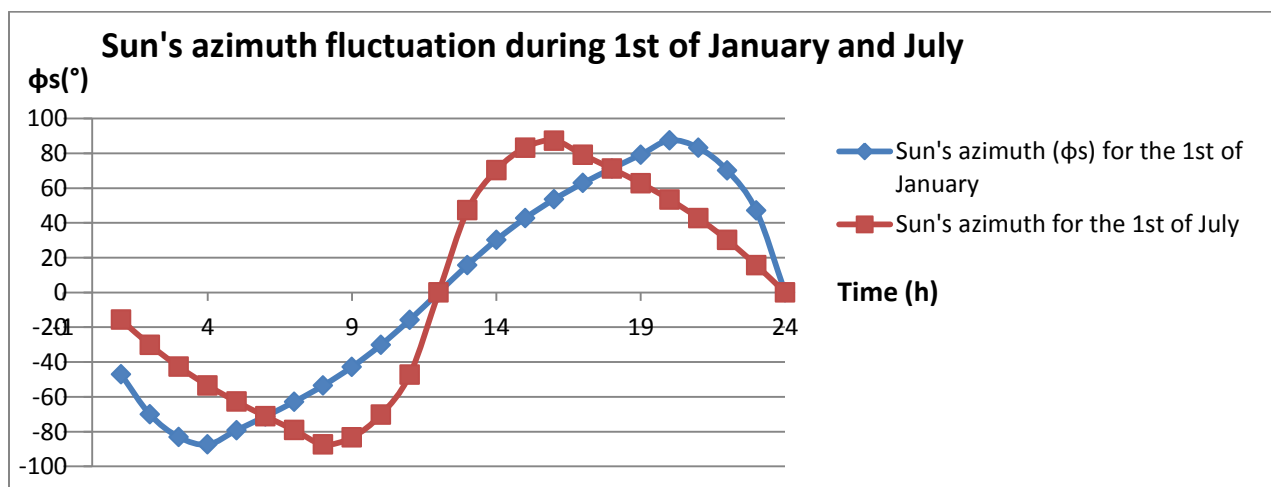


Figure 17: Sun's azimuth ( $\phi_s$ ) fluctuation during 1st of January and July



Analyzing the obtained sun azimuths of figure 17 it is obvious that before solar noon the values are negative and right after, they become positive and start increasing. During winter (blue line)  $\phi_s$  increases analogical as hours pass by till solar noon. The growth continuous with the same rhythm until 20:00pm when the peak of  $90^\circ$  is reached. Then a steep decrease takes place, which leads to the bottom down level of  $-90^\circ$  at 04:00am. As far as summer time is considered, the only depicted differences concern the increased rhythm of  $\phi_s$  after 08:00, which is steeper compared with January and the decrease time which starts sooner, around 16:00pm.

- **Cos( $\theta$ )-incidence angle**

Since all the unknown parameters have been obtained,  $\cos(\theta)$  can be estimated. In the following graph (Figure 18) the fluctuation of the incidence angle during a typical winter and summer day will be presented.

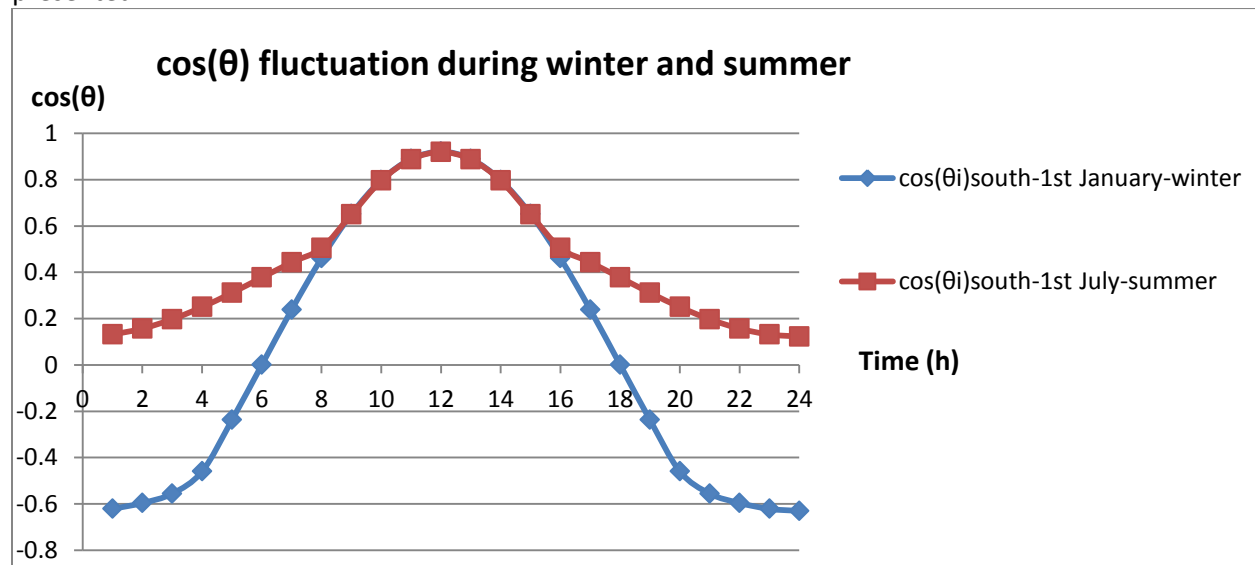


Figure 18:  $\cos(\theta)$  fluctuation during winter and summer days

According to the graph (Figure 18) during winter the cosine of the incidence angle increases sharply after 01:00 am and becomes positive after 06:00am. Afterwards, it continues increasing reaching the peak at 12:00am. Then a progressive symmetric decrease follows until 18:00pm, when it starts taking negative values. On the other hand, during summer  $\cos(\theta)$  is positive for the whole part of the day. The sequence of both graphs is similar, revealing only different bottom down points.

- **Rb parameter**

On figure 19, the factor  $R_b$  is depicted in an hourly base during the 1<sup>st</sup> day of January and July.  $R_b$  is unitless and it is used for the determination of Tilted beam irradiation ( $R_{bt}$ ). The fluctuation of  $R_b$  differs quite significantly depending on the given orientation. As it was explained above  $R_b$  equals with the ratio of incidence angle of beam irradiation and the zenith angle of the sun per hour of the day.

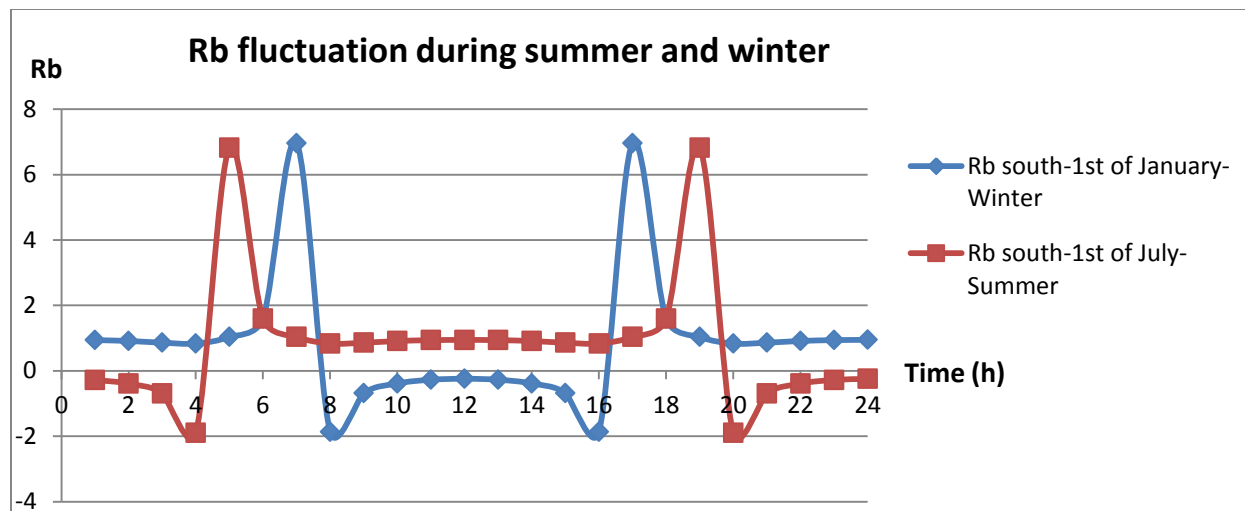


Figure 19: Rb fluctuation during summer and winter

On figure 19 the difference of Rb values is presented between a typical winter and a typical summer day. During winter Rb remains relatively steady until 05:00am, when a steep increase takes place reaching the peak level of 7 at 07am. Afterwards, an equally steep decrease follows leading to the bottom down value of -2 around 08:00 am. Furthermore, Rb increases slightly remaining negative until 15:00pm, when once more is suddenly dropped down to the bottom down point of 5. This sudden decrease is followed by a vertical increase to the peak at 17:00pm and a steep decrease to 1 at 18:00pm, which remains until the end of the day. On the other hand, Summer is characterized by similar ups and downs with different frequency. The peak value of Rb during July is around 7 at 05:00, whereas bottom down value of -2 takes place at 04:00am and 20:00pm respectively.

Since all the unknown parameters are calculated or obtained, equation 6 of methodology part can be implemented for the estimation of the tilted beam irradiation. The results can be seen on Figure 20.

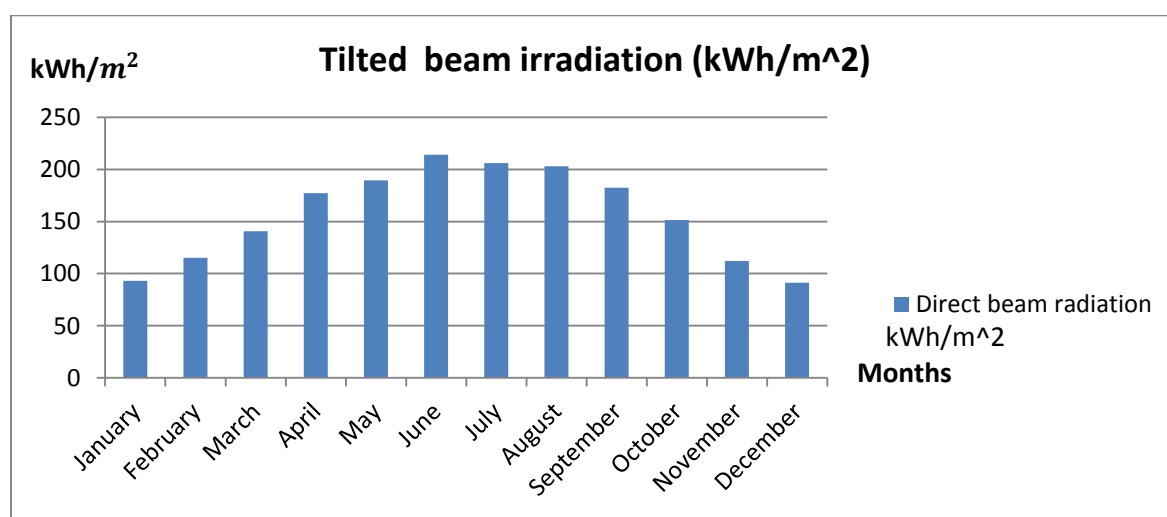


Figure 20: Tilted beam irradiation for South orientation

According to figure 20 the total monthly tilted beam irradiation for the South orientation fluctuates between the lowest level of  $91\text{kWh}/\text{m}^2$  on December and the peak of  $214\text{kWh}/\text{m}^2$  on June. The increase from January towards is quite steady, revealing once more that during Summer irradiation's level is by far higher compared with the other seasons. This was expected also from the graphs of diffused and reflected irradiation, which were similar (Figure 15) appearing huge increase as well. After June a steady decrease revealing winter's entrance takes place, when December irradiation drops down to  $91\text{kWh}/\text{m}^2$ .

Implementing equation 16 and summing up all the three components of tilted irradiation, the total daily monthly and yearly tilted irradiation was calculated. On figure 21 below, the monthly obtained results are depicted.

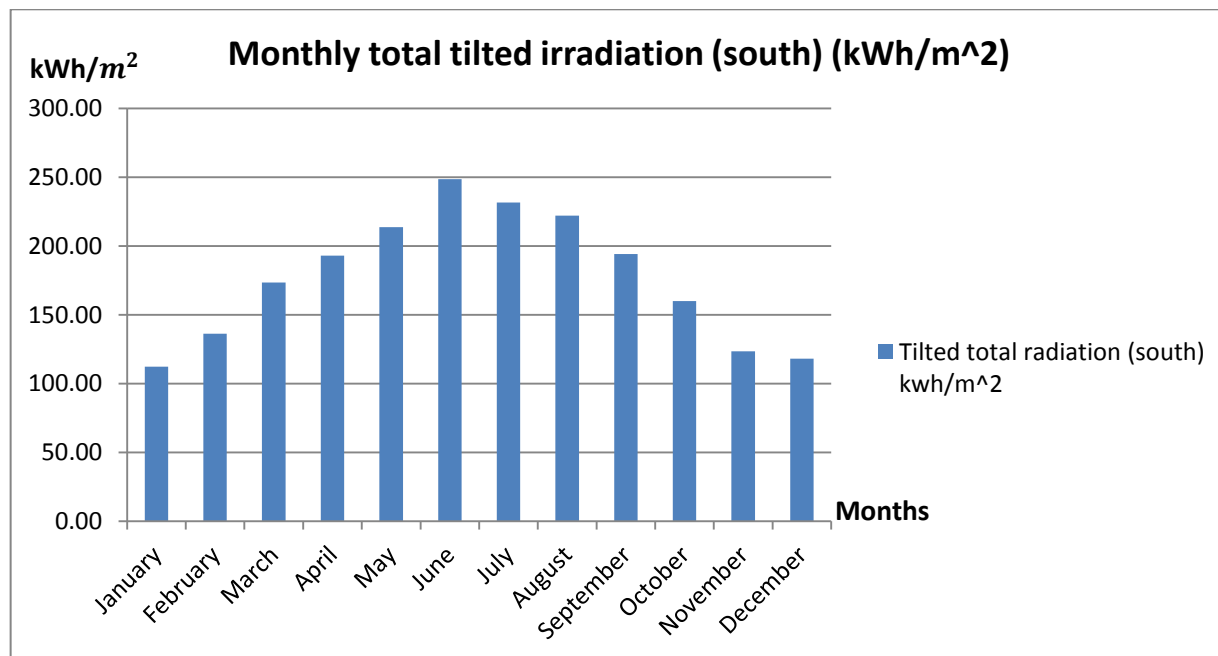


Figure 21: Monthly total tilted irradiation in  $\text{kWh}/\text{m}^2$

The presented results reveal that the total yearly received irradiation in an incline surface of  $37^\circ$  will be around  $2074\text{kWh}/\text{m}^2$ . Comparing the obtained results with Figure 10, it is concluded that the tilted surface receives more irradiance than horizontal surface by 19.6%. The quantity of irradiation starts increasing from January towards reaching the peak during June ( $250\text{kWh}/\text{m}^2$ ). During July and August the received irradiation will remain high at the level of  $232\text{kWh}/\text{m}^2$  and  $222\text{kWh}/\text{m}^2$  respectively. December and January belong to the lowest received irradiation months similarly with all the previous graphs. The average monthly irradiation value is  $177.16\text{kWh}/\text{m}^2$ .

## 7.5. PV panels expected produced energy yield

At this chapter, the expected energy yield of the PV installation will be estimated. In contrast with the previous sections, the modules characteristics will be inserted into the research study obtaining a key position. For the prediction of the produced energy, the next steps will be followed.

- **Steps**

1. According to equation 17 (CANMET, 2001-2004) the average efficiency of each PV array equals with:

$$17. np = nr[1 - \beta p(Tc - Tr)]$$

Where,

- The PV panels maximum theoretical efficiency  $nr$  equals with 19.4% (Sunovation, 2015).
- The temperature loss coefficient  $\beta p$  equals with 0.42%/°C (Sunovation, 2015).
- The temperature  $Tc$  has been calculated using equation 18.

$$18. Tc - Ta = (219 + 832\overline{Kt}) \frac{NOCT-20}{800}$$

- In order  $\overline{Kt}$  to be calculated the average data of extra-terrestrial irradiation between 2000-2005 were downloaded using SODA in hourly basis (Clive Best, 2005). Thereafter, the daily average Global Horizontal irradiation was divided with the daily average extra-terrestrial irradiation  $H_0$ . The results can be seen on Figure 22.

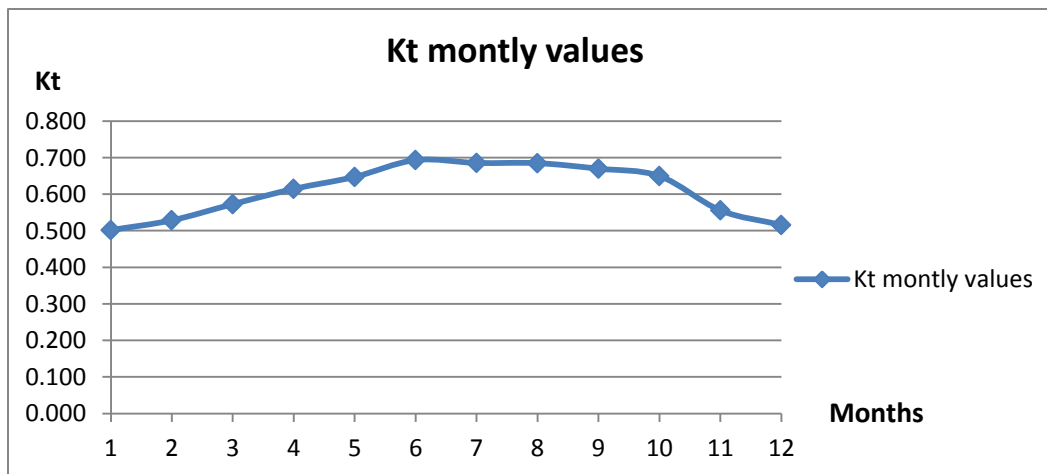


Figure 22: Kt montly fluctuation

Observing the values of figure 22, it is noticed that Clearness Index( $Kt$ ) fluctuates slightly during the year. As colder the weather is, the lower it's value will be. During winter (December-February)  $Kt$  varies among (0.502-0.529). This means, that only 50.2% to 50.9% of the extra-terrestrial irradiance is absorbed from earth's atmosphere and it's not reflected or diffused back. Contrary, during summer time irradiation's absorption is significantly higher leading to values such as 69.3% on June.



- Nominal Operating Cell Temperature (NOCT) is 56°C (SUNOVATION ANEX (Sunovation, 2015)).
- $T_a$  was calculated taking into consideration only the daylight values of temperature for the whole year. The reason for the isolation of the daylight temperature is that the PV panels are not operating during the night due to lack of irradiation. Therefore, if night's temperature is included then the results will not be quite reliable. The data were given from the National Observatory of Athens (noa.gr, 2015). On table 5 the monthly average temperatures of 2014 will be presented.

Months	Mean monthly average daylight temperature $t_a(^{\circ}\text{C})$
January	15.9
February	15.7
March	16.3
April	18.9
May	22.1
June	26.5
July	28.3
August	29.6
September	26.4
October	22.6
November	18.7
December	17.7

Table 6: Mean monthly daylight temperature

According to table 6, the temperature variation among the year of 2014 is quite high. February is the coldest month when the average daylight temperature drops down to 15.7°C. On the other hand, a temperature increase is noticed as summer approaches reaching the peak during August when the thermometer almost touches the level of 30°C. In this point, it should be written that there are some summer days where the temperature overpass even 40°C leading to dangerous consequences for people's health such as heat strokes. Moreover, the risk of fire increases vertically when desert temperatures are accompanied with strong winds setting at risk the last green lungs of Greece's forestry.

- Since all the above parameters have been obtained, temperature ( $T_c$ ) must be multiplied with the correction factor ( $C_f$ ), which will be calculated using equation 20 (CANMET, 2001-2004). This step takes place, due to the fact that the installed PV panels will be fixed in an optimal average position, however the hourly sun's fluctuation leads to losses. In case of sun's tracker installation for the following of sun's path then  $C_f$ 's calculation wouldn't be necessary. ( $T_c$ ) and ( $C_f$ ) were calculated in an hourly base for the whole year and the monthly average will be presented.

Months	T <sub>c</sub> (°C)	C <sub>f</sub>
January	42.29	0.95
February	44.41	0.98
March	47.56	1.00
April	51.20	0.99
May	53.85	0.96
June	58.41	0.94
July	60.47	0.95
August	63.73	0.98
September	61.30	1.00
October	56.14	0.99
November	47.28	0.96
December	43.96	0.94
Yearly average	52.55	0.97

**Table 7: Panels temperature (T<sub>c</sub>) and correction's factor (C<sub>f</sub>) monthly fluctuation**

Observing C<sub>f</sub> variation, it is noticed that the values of the correction factor are close to 1. The reason why that phenomenon takes place is the average optimal inclination of the panels. According to table 5 C<sub>f</sub>'s range fluctuates in-between 0.94 on December and 1 during September and March. To be more specific, correction's factor value starts increasing analogically from December to March when it reaches the peak of 1, followed by a similar decrease until June, when (C<sub>f</sub>) touches the bottom down point of 0.94. Afterwards, it is increasing again until September when it becomes again 1 and starts decreasing towards with the same rhythm till December. The average value of (C<sub>f</sub>) among the whole year is 0.97.

As far as panels temperature (T<sub>c</sub>) is considered, (T<sub>c</sub>) is dependent entirely on the environmental temperature. As higher the outside temperature is the higher the panels temperature as well. January consists the bottom down month of (T<sub>c</sub>), when it's dropped down to 42.29°C. However, as months pass by approaching to summer, it starts increasing significantly reaching the peak of 63.73°C on August. The yearly average of (T<sub>c</sub>) is 52.55°C.

Since the Nominal Operating Cell Temperature (NOCT), the maximum theoretical efficiency (n<sub>r</sub>), the daylight hourly temperatures (T<sub>a</sub>), the PV panels cell temperature (T<sub>c</sub>) and the reference temperature (T<sub>r</sub>) are estimated, the modules hourly efficiency (n<sub>p</sub>) can be calculated implementing equation 17. The monthly average values are presented on Figure 23.

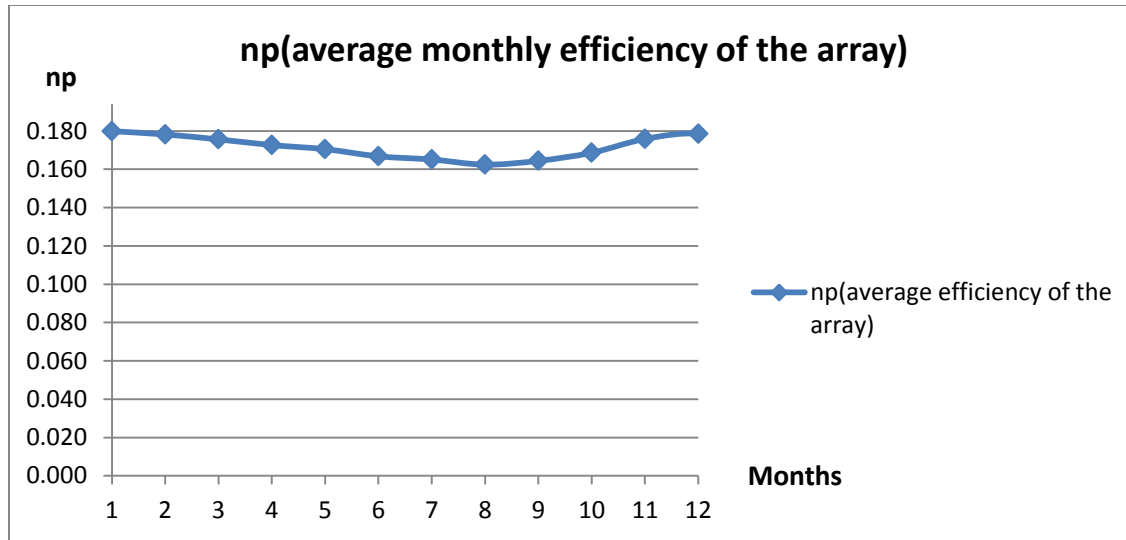


Figure 23: Average monthly panels efficiency( np) fluctuation

The results which are depicted on the graph above (Figure 23) reveal that the maximum theoretical efficiency of 19.4% is never reached. However, it is noticed that during winter, efficiency values reach 18% and they are depicted as the most efficient months. Moreover, it is observed that as closest the panels temperature to the reference is, the higher the performance of the modules. During summer efficiency fluctuates among 16% and 17% leading to 8%-10% decreased performance in comparison with winter. The top down value of 16.2% takes place on August, when the panels temperature ( $T_c$ ) reaches the highest level of 63.73°C.

Taking into consideration all the above parameters, the monthly energy produced from the PV arrays will be presented on the following figure 24. The results were based on equation 21 of methodology's part (Shahnawaz Farhan Khahro, 2014), where the total energy yield is depending on the total PV surface, the monthly efficiency and the sum of Tilted irradiation.

$$21.E_p = Snp\overline{H\tau}$$

The total surface area ( $S_n$ ) was calculated to be  $63610m^2$  from section 7.3, the efficiency's average monthly values (np) are depicted on Figure 23 and the summed up tilted irradiation ( $H_t$ ) in an inclined surface of 37° is presented analytically on Figure 21.

Furthermore, the produced energy is accompanied with miscellaneous and power condition losses such as ohmic losses, soiling losses etc. which were depicted in the methodology part, but they will be presented once more, even more detailed on table 8 (Sunovation, 2015).

Miscellaneous and power conditioning losses	Losses in %
1) Shadings	0.0%
2) Losses due to weak radiation	5.0%
3) Losses due to dust and snow	2.0%
4) Module array mismatch losses	2.0%
5) Mismatch efficiency losses	2.5%
6) Inverter losses	1.5%
7) Ohmic wiring losses	0.90%
8) Incident effect losses	4.10%
9) Module quality losses	1.10%

Table 8: Miscellaneous and power conditioning losses of the PV modules

According to Sunovation's brochure, from which all the losses data were retrieved, it is noticed that the higher losses percentages are linked with the weak irradiation, where they overpass 5%. All the other losses categories fluctuate among 0.9 and 2% with the exception of incident effect losses which equal with 4%.

On figure 24 below the produced energy yield from the Photovoltaic park of Pserimos will be presented with and without the expected losses.

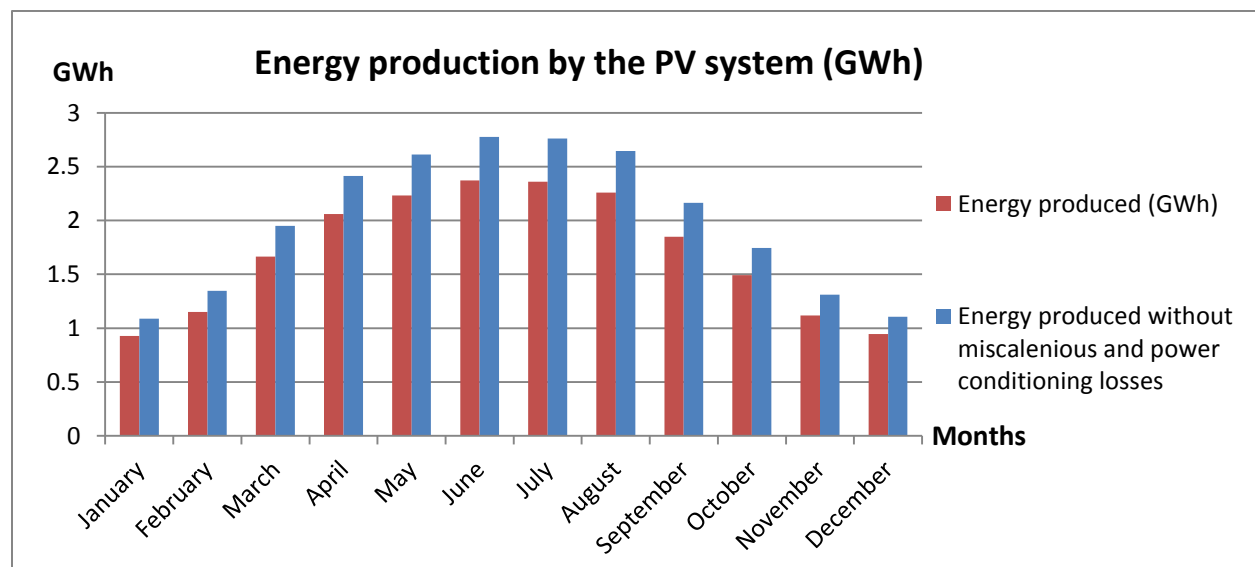


Figure 24: Energy produced with and without miscellaneous and power conditioning losses

- **Energy produced taking into account all the intermediate losses (red graph)**

According to figure 24, the expected monthly energy production taking into account all the intermediate losses (red graph) for the conversion of irradiation to electricity will fluctuate between 0.93GWh and 2.37GWh. The top down values of 0.93GWh and 0.94GWh take place during January and December respectively due to reduced irradiation levels. On the other hand, as the summer approaches the irradiation increases significantly with progressive rhythm leading to the parallel growth of energy





production. The peak value is achieved on June, when the energy yield reaches the amount of 2.37GWh. After July a similar decrease of energy is noticed, roughly estimated to be around 0.3GWh per month. The total energy produced from the PV system is expected to be **20.43GWh per year**.

- **Energy produced without taking into account the intermediate losses (blue graph)**

As far as the total energy yield without taking into account the intermediate losses is considered (blue graph), the expected monthly energy would be 23% higher. The peak value would be achieved during June and it would reach the amount of 2.77GWh. Contrary, the bottom down level would take place during January and December identically with the red graph and it would be 1.1GWh. The total yearly energy production would be 23.92GWh.

Of course the realistic scenario is the first one (red graph) and the blue graph of Figure 24 describes a potential future case where technological development is highly evolved and losses are almost neglected.

## 7.6. PV system's total efficiency calculation

In this section the total efficiency of the PV system will be calculated. The realistic sun to used electricity efficiency is quite different than the given one of 19.4% retrieved from Sunovation. The reason is that the losses from electricity's transportation as well as all the intermediate losses such as described on table 8 are not taken into consideration. For the estimation of the total efficiency, equation 23 was used and the results are depicted on table 9.

Months	nA(south)
January	0.155
February	0.143
March	0.139
April	0.138
May	0.136
June	0.132
July	0.129
August	0.127
September	0.133
October	0.138
November	0.142
December	0.155
Years Average	0.139

Table 9: The monthly efficiency of the PV system

According to the results depicted on table 9, the maximum PV system's efficiency is not overcoming the level of 15.5%. During winter, efficiency varies among 14.3% and 15.5%. However, as the temperature increases, efficiency decreases respectively. In this case the efficiency is 23% lower than the no losses scenario.

## 8. RESULTS (Wind park part)

### 8.1. Wind speed estimation

The wind speed data were gathered from a wind logger installed in Cos airport, 7 miles away from the research location. All the wind speed data were retrieved from the national observatory of Athens in 10 minutes step for the whole years of 2013 and 2014 (meteo.gr, 2015). The first depiction concerns the wind dynamic at 10m height (wind sensor height) revealing the average fluctuation of both obtained years.

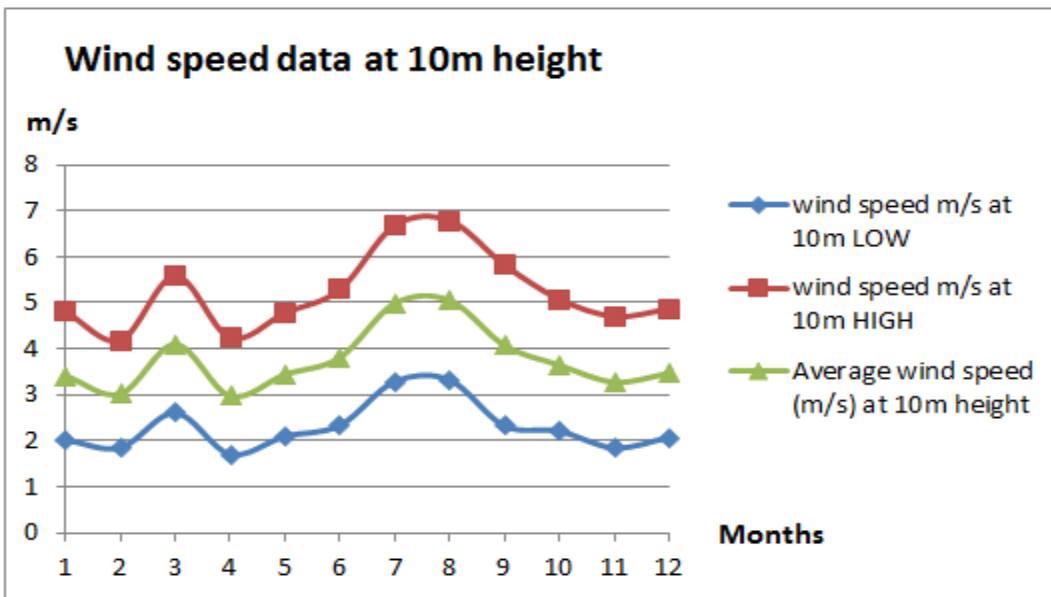


Figure 25: Wind speed measurement data at reference height (10m)

On the above graph (Figure 25) the monthly average wind speed fluctuation is presented. The blue highlighted graph shows the lowest levels of wind that were recorded revealing that the wind speed is lower than the cut-in limit that is needed for the wind turbines operation. Only during July and August the wind speed level is slightly higher compared to the cut-in limit of 3m/s (Vestas, 2015). On the opposite side, the red highlighted graph depicts the highest level of monthly wind dynamic that occurs, showing a minimum of 4m/s during February and April, whereas the maximum value reaches the size of 7m/s during July and August. For better data processing, the mean wind speed values were calculated (green graph), revealing a year's average of 3.8m/s and a monthly variation between 3m/s (February-April) and 5m/s (July–August).

In this case though, the measurement took place in the wind sensors height which equals with 10m (meteo.gr, 2015), therefore it is not realistically representative. The main reason for that is the exponential growth of wind dynamic as height increases (Ioannis Fyrippis, 2010). In order to predict the growth of wind speed at 95m, which is the wind turbine's hub height, the power law equation (equation 25 of methodology) will be implemented (Touma, 2012).

$$25. U_2 = U_1 * (Z_2/Z_1)^a$$

Using equation 26 of methodology, parameter  $\alpha$  was calculated and equals with 0.138. Moreover, Z2 which represents hub height is known from Vestas brochure and equals with 95m, whereas the reference measurement height is 10m. Based on the above data and the wind speed recorded at the reference point, the wind speed at hub height was estimated.

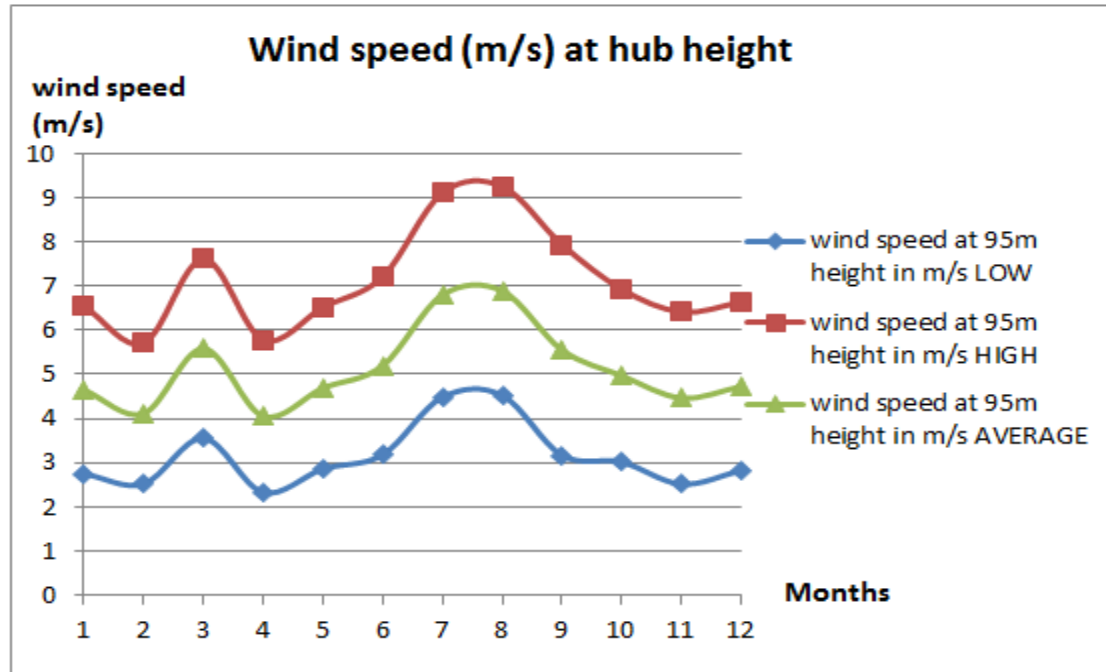


Figure 26: Wind speed data at hub height (95m).

On figure 26 the wind speed fluctuation among the year at hub height of 95m is presented. According to the resulted graphs, the average monthly wind speed (green graph) varies between 4m/s and 7m/s. The bottom down values were observed during winter, when the average wind speed was dropped down to 4.7m/s. On the other hand, summer was possessed from considerably stronger winds revealing an average of 6.3m/s, increased by 28.5 % compared with winter's period. Moreover, during spring and autumn the average speed reached the level of 4.5m/s and 5m/s respectively. The year's average is 5.14m/s making the wind installation technically feasible for operation.

The wind's direction tends to fluctuate among the year, however it presents higher frequency from the West side covering the 23.4% yearly. Afterwards, West-North West and West-South West directions are following with 16.5% and 15% respectively. According to the results of table 10, the 55% of the incoming wind to Pserimos is mainly West directed, defining West as the most suitable location for the wind turbines installation. The remaining 45% is consisted of south winds (19%), north winds (17.2%) and east winds (8.8%).

Wind direction	Yearly Percentage (%)
N	1.67
NNW	5.1

NW	9.4
NNE	0.69
NE	0.69
S	4.6
SSW	3.9
SW	2.9
SSE	4.1
SE	3.7
E	5.5
ENE	0.54
ESE	2.7
W	23.4
WNW	16.5
WSW	15

Table10: The frequency of wind blowing direction in Pserimos

Table 10 presents the yearly percentage of wind direction. The less frequent wind blowing direction it seems to be the East one, where coupled with East-North East and East-South East directions consist the 8.8% of the year's total. Furthermore, North direction winds consist the 17.2%, as it was aforementioned previously, whereas South direction winds, from which of them the most dominant ones are South and South-South East consist 4.6% and 4.1% respectively. The most frequent wind direction is West, where it represents the 55% of wind direction through the year.

On the following figure, the monthly distribution of wind's direction is depicted. According to the developed histogram the percentage of wind blowing monthly per orientation is presented revealing the most dominant winds per season.

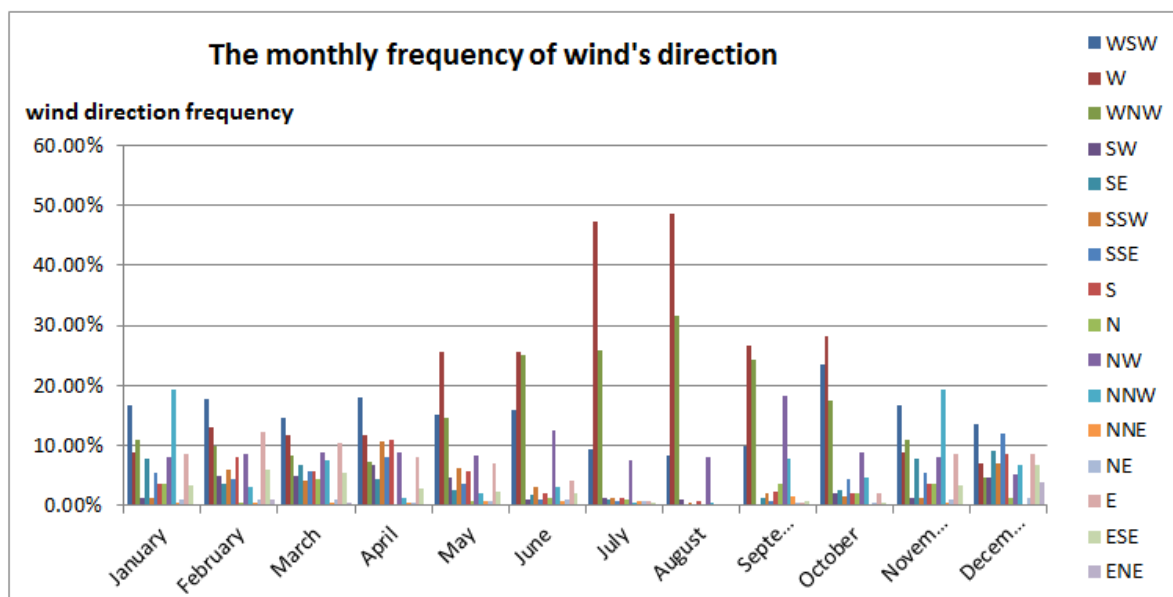


Figure 27: The monthly frequency of wind's direction

According to figure 27, January is characterized mostly from North-North West and West-South West directed winds, where coupled cover the 37% of the monthly wind currents. During February, March and April the incoming wind is more balanced, showing a slight tend to the West -South West and West direction. From May to August, West directed winds cover almost 50% followed by North winds, which fluctuate around 25%. Only during June an almost equal amount of West and North winds takes place covering 50% of month's total. September is characterized once more from West and North directed winds possessing the 26% and 24% of the total respectively. However, the level of North West direction is highly increased as well reaching 18%. The dominance of West directed winds ends when winter approaches, where North-North West and West-South West currents takes the first and second place respectively. As far as winter is considered, the variation of wind's direction is high, therefore the percentage is much more balanced compared to Summer.

## 8.2. Wind park location identification

Since the wind speed data were processed and the average year's value of 5.14m/s was considered as technically viable for wind turbines installation, the next step is the selection of the most appropriate locations of Pserimos for wind turbines placing.

Firstly, the direction of the wind turbines must be estimated according to the most dominant winds on the island. Since, it was found that the wind dynamic is characterized by West directed winds conceiving the 55% of the total share, then the wind turbines must be placed facing West. However, taking into consideration the average wind angle of all months, in order to place the wind turbines in a position which will cover all cases of wind direction, the exact facing angle of wind turbines must be 250°(West-South West) (Ioannis Fyrippis, 2010).Based on that, all the intermediate factors must be calculated maintaining this parameter stable.



Figure 28: Pserimos

On figure 28, the cardinal points compared to Pserimos are depicted (Google Earth, 2015). The north stands to the upper point of the island facing Turkey's coastline, whereas south targets Cos. Similarly with the north, east side is also neighboring with the Turkish borders desisting 12km from Karabag's city. As far as west side is considered, in a distance of 2.5km a small inhabitant islet is located, which is called Plati and 5km further the island of Calymnos takes place (Google Earth, 2015).

Moreover, in the bottom down left point of the map a green schematic is presented. The schematic represents the horizon spots, substituting them with their relative angle. The red arrows show the direction of 250° (West-South West), which is the average wind direction through the year and it will be used as reference point for wind turbines placing.

### 8.2.1. Wake effect

For the proper placing of wind turbines and the estimation of the in-between them distances the most important parameter that must be examined is the wake effect (F.Gonzalez-Logatt, 2012). According to this phenomenon, the wind leaving the turbine must have a lower energy content than the wind upstream of the turbine. As a consequence, the wind downstream of a wind turbine has reduced speed and is turbulent; this downstream wind is the wake of the turbine. As the wind flow proceeds further downstream this wake will begin to spread and gradually return to free stream conditions. If a wake intersects with the swept area of a downwind turbine, the downwind turbine is said to be shadowed by the turbine producing the wake. In that case the energy output of the shadowed wind turbine will be significantly lower leading to decreased wind park performance and the created turbulence will be responsible for causing blade damages to the turbine reducing its lifetime (F.Gonzalez-Logatt, 2012).

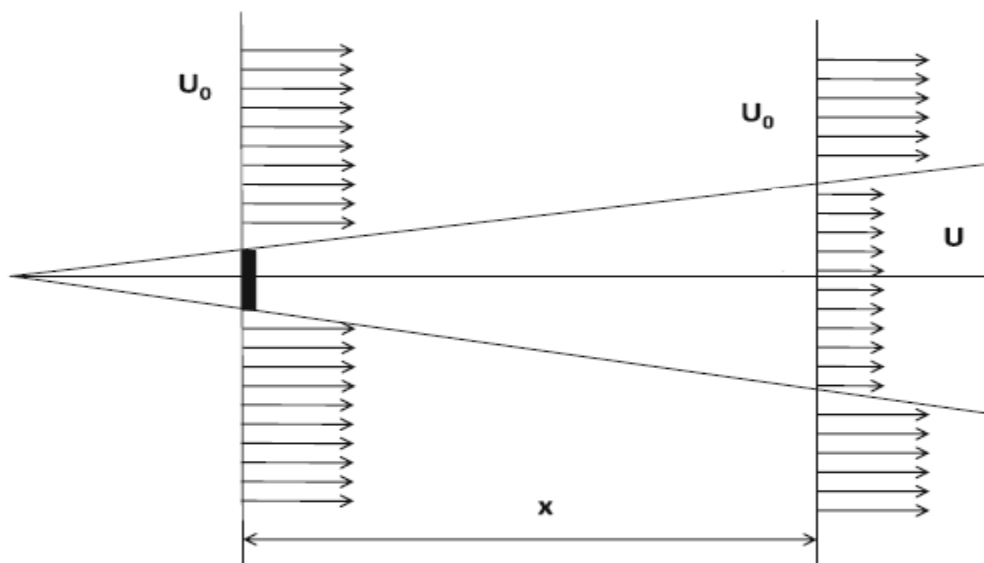


Figure 29: Wake effect

On figure 29 the flow of the wind before and after the interaction with the wind turbine is presented. If the upstream wind speed is  $U_0$ , when the wind interacts with the wind turbine, a turbulent downstream is developed characterized by reduced speed in the back side of the turbine. This stream expands in a

conic shape such as figure 29 reveals (Pardalos, 2013). The downstream wind speed  $U$  in the affected area is highly influenced from the distance that intercedes between the wind turbines. As closer to the turbine the higher the developed wake effect and the lower the wind speed. Therefore, the proper spacing between the placed wind turbines must be estimated in such way that their performance will remain as undisturbed as possible.

According to Ragheb, the most ideal distance between 2 turbines, in order to avoid the wake effect should be as far as possible from each other, however the land use and the increased financial expenses of connecting the turbines through cabling to the electrical grid makes this process economically inefficient (M.Ragheb, 2015). Therefore, the following separating distances have been established:

- 4 times the hub height apart perpendicular to the prevailing wind direction (M.Ragheb, 2015).
- 7 times the hub height apart horizontally with the wind direction (M.Ragheb, 2015).

By implementing the above separating distances in the wind park installation then the developed wake effect in-between will be quite decreased, but not completely dissolved, therefore the power loss of each wind turbine separately must be estimated.

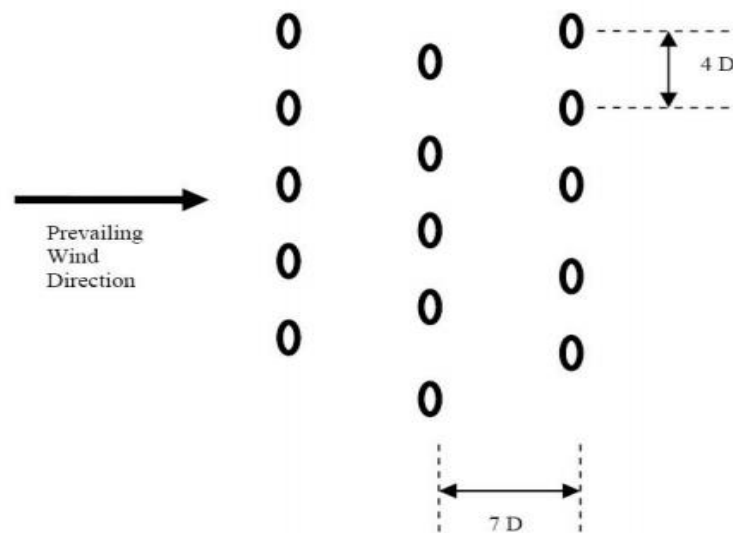


Figure 30: Proper wind turbines placing

On figure 30, the most preferable distances perpendicular and horizontal to the wind are depicted, whereas distance ( $D$ ) represents the hub height of the turbines (Pardalos, 2013). According to the schematic, the turbines behind the first array are placed in the middle of the created gap in between the front line. The reason for that is the reduction of the wake that affects the downstream wind turbines.

Based on the above data, the distances between the wind turbines in Pserimos must be **380m** apart perpendicular with the wind direction and **665m** apart horizontal to the wind direction. Additionally, the altitude must be taken into consideration as well as the potential obstacles that block or influence the upstream wind currents.



### 8.2.2. Wind speed decrease due to Wake's effect

Since the distances between the wind turbine arrays have been calculated, the wind speed decrease resulted from wake effect that will affect the produced output of the arrays behind the first one can be estimated. For the calculating procedure Jensen model will be implemented and the necessary steps are presented below (M.Ragheb, 2015).

- **1<sup>st</sup> step:** scalar (a) determines how quickly the wake expands with distance and it is defined as:

$$32.a = \frac{0.5}{\ln(\frac{z}{z_0})}$$

Where,

- Z represents hub height (m)
- Zo represents the surface roughness (m)

The surface roughness equals with 0.32 for Pserimos morphology (Katsaprakakis, Wind energy, 2007) whereas hub height is known, therefore scalar a can be calculated and equals with 0.43.

- **2<sup>nd</sup> step:** The axial induction factor ( $\alpha$ ) must be estimated and it's computed by the following expression:

$$33.\alpha = 0.5 * (1 - \sqrt{1 - Ct})$$

Where,

- Ct represents the thrust coefficient which equals with 0.88 according to Vestas (Vestas, 2015).

By substituting the thrust coefficient with 0.88 then the axial induction factor equals with 0.325.

- **3<sup>rd</sup> step:** The downstream rotor radius rd must be calculated as well and equals with:

$$34.rd = rr * (\frac{1-\alpha}{1-2\alpha})$$

Where,

- rr represents the radius of the rotor (m)

The radius (rr) can be calculated since the diameter of the rotor is 100m according to Vestas, whereas the factors (a) and ( $\alpha$ ) are already estimated from equations 32 and 33 respectively. Implementing equation 34 rd is found to be equal with 93m.

- **4<sup>th</sup> step:** The final step is the calculation of the velocity deficit induced on position (j) which is the location of the wind turbines behind 1<sup>st</sup> array because of the wake generated by (i) (1<sup>st</sup> arrays position).

$$35.Vdij = \frac{2*\alpha}{1+a*(\frac{xij}{rd})^2}$$

Where,



- $x_{ij}$  represents the intermediate distance of both wind turbines (m)

With the implementation of equation 35 the percentage of velocity's decrease will be estimated taking into consideration the scalar, the axial induction factor and the distance between the turbines. By replacing all the above parameters with their calculated values it was concluded that the wind speed which inserts the blades of the second array will be reduced by 2.7%. The same wind speed drop will occur also in the arrays behind the second one since the intermediate sitting distances are similar.

### 8.2.3. Hill speed up effect

A quite common approach for wind turbines installation is to position them on the edge of a hill, ignoring the surrounding landscape. The main reason for that is that the exposure to the prevailing winds is significantly higher. Moreover, it is observed that on the hills the wind speed is increased due to the fact that the wind becomes compressed on the side of the hill facing the wind and when it reaches the top and spills to the other side it can expand again in the low pressure area on the lee side of the hill. The decreased static pressure is linked with a growth of the kinetic pressure obtained from Bernoulli's equation, which leads to increased wind speed. The smoother with hemi-cylindrical shape the hill is, the better location for turbines installation (M.Ragheb, 2015).

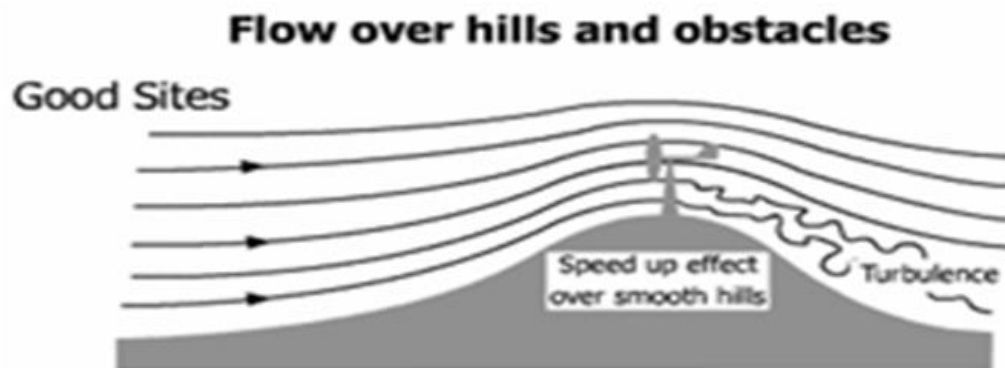


Figure 31: Wins flow when passing over a hill

On figure 31 the speed up effect of the wind on a hill is described. The wind due to compression increases its speed on the top of the hill, influencing positively the energy output produced by the turbine (M.Ragheb, 2015). Afterwards turbulence is developed on the downstream wind current as a consequence of the irregular hill's surface coupled with the wind turbine's blades movement.

### 8.2.4. Tunnel speed up effect

Except hill's speed up effect there is also another phenomenon that increases the spot wind speed compared with the neighbor area and it's called tunnel speed up effect. This case refers to the acceleration of the wind speed when the wind current flows through the created gap of two mountains.

During this situation the mass of air becomes compressed relative to the size of the existent gap and it can be explained using Bernoulli's equation 36 (M.Ragheb, 2015):

$$36. p_1 + \frac{1}{2} * \rho * V_1^2 = p_2 + \frac{1}{2} * \rho * V_2^2 = \text{constant}$$

Where:

- $\rho$  represents air density in  $\text{kg/m}^3$
- $V_1$  represents the upstream wind speed in  $\text{m/s}$
- $V_2$  represents the wind speed influenced by the tunnel effect in  $\text{m/s}$
- $P_1$  represents the upstream wind's pressure
- $P_2$  represents the wind's pressure in-between the gap of the two mountains

The above equation can be written also as:

$$V_2^2 = \frac{2}{\rho} * (p_1 - p_2) + V_1^2$$

Which means that if  $P_1 > P_2$  then  $V_2 > V_1$

Additionally, the continuity equation 37 shows that the smaller the area in-between, the higher the increase of the wind speed.

$$37. \rho * A_1 * V_1 = \rho * A_2 * V_2$$

The air density  $\rho$  remains stable, therefore only wind speed  $V$  and the intermediate space  $A$  will be influenced respective with the given circumstances.



Figure 32: Wind turbine takes advantage of tunnel effect

On figure 32 a digital illustration of a wind turbine positioned inside two mountains is presented. The turbine is installed in that spot, in order to take advantage of the tunnel effect and the increased incoming wind speed which will result in higher performance.

In this case study the level of wind speed increase which was induced by hill's and tunnel's speed up effect is impossible to be estimated due to lack of pressure data for the research location. The described effects will only be used for the selection of the most favourable installation spots.

### 8.2.5. Wind turbines sitting spots selection

The spot selection was based on the most potentially favorable wind speed locations on the island influenced by hill's and tunnel's speed up effect. Moreover, the distances in-between the wind turbine arrays were estimated according to Rayleigh article, taking into consideration the consequences of the turbulence flow and the wake effect.



Figure 33: Wind turbines location

On figure 33 the selection points for the wind turbines installation are presented. The first string which is consisted of the wind turbines 1 to 5 is located on the South part of the island. There is only one turbines array on that spot due to land limitations, whereas the in-between distance of the placed turbines is roughly 380m (4D). The wind turbines was decided to be installed on the edge of a rounded hill, considering that spot as the most favorable for increased wind speed currents due to the developed hill's speed up effect.

The second turbines string is located on the South-West part of Pserimos and it's consisted of 3 wind turbines (6-7-8). Wind turbines 6 and 8 are positioned on the top of a smooth hill taking advantage of the hill's effect, whereas turbine 7 is installed in-between the two aforementioned hills where the

tunnel effect dominates resulting to increased wind speeds as well. The morphology of the area didn't allow the installation of more wind turbines vertically, due to decreased altitude conditions (Google Earth, 2015). In case where more wind turbines were installed behind 6, 7 and 8 then they would be shadowed, suffering from turbulence flows due to the higher altitude mountains sited in front of them facing the average wind direction.

The third string is consisted of the wind turbines 9 to 14, which are located in the North-West side. In this case the installation spot was selected based on the hill's speed up effect, targeting to increased energy output once more. Furthermore, the range of the turbines could not overcome the depicted number due to Greek's legislation which forbids wind turbines installation in a distance closer than 500m from any residential area (ypeka.gr, 2015).

Vertically behind the third string, one more array was decided to be installed in a distance of 660m (7D) cause the altitude of the surface allows it. The 4<sup>th</sup> array is positioned in an altitude of 130m (Google Earth, 2015), slightly higher compared to the 3<sup>rd</sup> array and it's consisted from turbines 15 to 19. The sufficient altitude coupled with the favorable distance away from the array in front, lead to decreased power losses due to wake effect's shadowing.

The last two installed turbines (20, 21), were sited in a smooth hill around 800m away from the 4<sup>th</sup> array, taking advantage of hill's effect. All the wind turbines are installed based on the mean wind direction facing West-South West side.

### 8.3. Air density

The next parameter that must be determined is the air's density fluctuation at hub height which varies slightly through the year. Air's density was calculated in a 10 minutes step for the years of 2013-2014 and it was based on equation 27 of methodology's part. According to equation 27 density depends on a variety of factors, where most of them are stable whereas only temperature fluctuates (Ioannis Fyrippis, 2010).

Stable factors	Values
hub height $z_2$ (m)	95
surface roughness $z_0$ (m)	0.032
standard air density $\rho_0$ ( $\text{kg}/\text{m}^3$ )	1.225
standard sea level temperature $T_0$ (K)	288
$\Gamma$ (K/km)	6.5
altitude above the sea $Z$ (m)	115
$R$ ( $\text{J}/\text{d}^*\text{K}$ )	287
gravity acceleration $g$ ( $\text{m}/\text{s}^2$ )	9.81

Table 11: Stable factors of air's density

On table 11 the stable factors that were used for density's calculation are presented. The hub height is known from Vestas brochure and equals with 95m (Vestas, 2015), whereas surface roughness for Pserimos surface morphology is considered to be 0.032m. Moreover, the standard sea level temperature is taken as 288K and the vertical gradient temperature  $\Gamma$  is usually assumed to be 6.5K/km

(Ioannis Fyrippis, 2010). Furthermore, the average altitude  $Z$ , where the wind turbines were installed is 115m according to Google's Earth software, however the actual altitude of the wind turbines operation equals with the sum of the surface altitude and the hub height. The gas constant  $R$  is known to be  $287 \text{ J/d}^\circ\text{K}$  and the gravitational acceleration  $g \text{ 9.81m/s}^2$  (Ioannis Fyrippis, 2010).

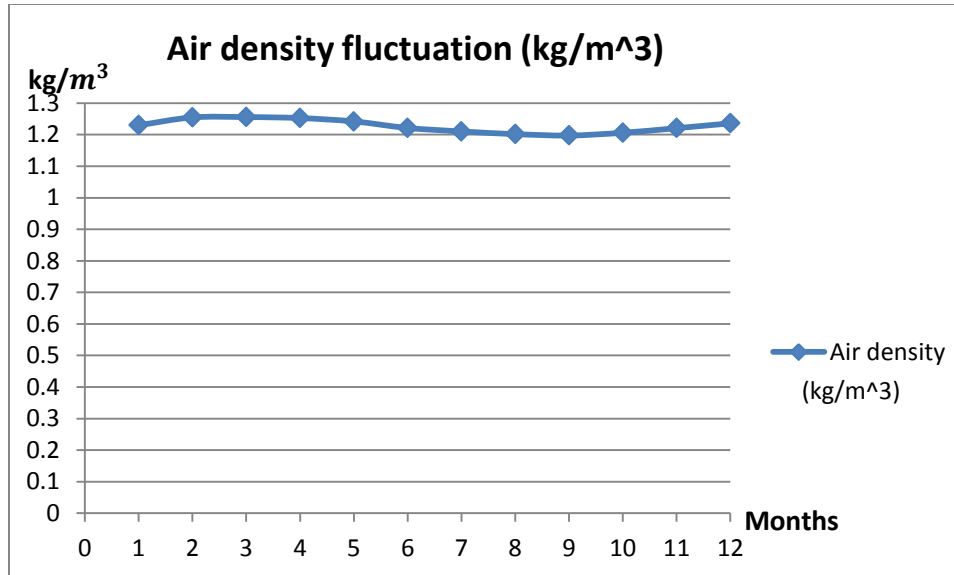


Figure 34: Air's density fluctuation at hub height

On figure 34 the mean monthly fluctuation of air density among the year is illustrated. The peak month of air density at hub height altitude is March when it reaches the level of  $1.26 \frac{\text{kg}}{\text{m}^3}$  followed by February with  $1.25 \frac{\text{kg}}{\text{m}^3}$ . In general, it is observed that the mean air density during spring is higher compared with the other seasons obtaining an average of  $1.25 \frac{\text{kg}}{\text{m}^3}$ , when during winter summer and autumn the mean season values are  $1.244 \frac{\text{kg}}{\text{m}^3}$ ,  $1.211 \frac{\text{kg}}{\text{m}^3}$  and  $1.208 \frac{\text{kg}}{\text{m}^3}$  respectively. The air is presented to be less dense during September, when the bottom down mean value of  $1.2 \frac{\text{kg}}{\text{m}^3}$  is achieved. During January air density is around  $1.24 \frac{\text{kg}}{\text{m}^3}$  and as the months pass by a slight progressive increase takes place until March when the peak value is reached. From April towards to September air's density starts decreasing in a similar rate dropping to the bottom down value of  $1.2 \frac{\text{kg}}{\text{m}^3}$ .



## 8.4. Technical characteristics of the selected wind turbine model Vestas V100-2MW

In this section the technical and operating characteristics of the selected wind turbine model Vestas V100-2MW will be presented and discussed analytically.

Technical characteristics	Values
<b>Operating data</b>	
Rated power(kw)	2000
Cut- in wind speed (m/s)	3
Rated wind speed (m/s)	12
Cut-out wind speed (m/s)	22
Performance coefficient $C_p$ (%)	42
<b>Rotor characteristics</b>	
Rotor diameter (m)	100
Swept area ( $m^2$ )	7854
<b>Blade dimensions</b>	
Length (m)	49
<b>Inverter characteristics</b>	
Inverter efficiency (%)	98.5

Table12: Technical characteristics of Vestas V100-2MW model

All the above gathered data were retrieved from Vestas (Vestas, 2015), which includes in detail all the technical characteristics of the specific model. The selection of a 2MW capacity turbine was based on the Europeans average of commercial wind power models according to windustry.org (windustry.org, 2014), whereas the specific type was chosen due to lower cut-in and rated wind speed compared to other 2MW turbines. According to table 12 the turbine starts to operate when the wind speed overcomes the value of 3m/s (cut-in wind speed), making the selected model appropriate for the studied location since the year's average is 5.14m/s. The rated wind speed (12m/s) is characterized as the bottom wind speed limit, where the turbine reaches peak production. In-between rated and cut out wind speed limits, the turbine remains on peak production mode, however when cut out limit (22m/s) is reached then blade brakes are activated stopping wind turbines operation for the avoidance of any potential damage.

Coefficient of performance ( $C_p$ ) determines the percentage of kinetic energy produced by the blade movement that will be converted into electricity (Libii, 2013). ( $C_p$ ) theoretically can reach the limit of 59% which is called the Betz limit, however this is not realistically representative since the average performance of commercial wind turbines fluctuates between 0.3 and 0.5 (Libii, 2013). The coefficient of performance is highly dependent on the existed wind speed, therefore it is not remaining stable during wind turbines operation but it varies within a predetermined range. According to Vestas V100-2MW technical characteristics this range fluctuates between 0.35 and 0.5 but for simplifying the calculation procedure the average of 0.42 will be used (Vestas, 2015).

Rotor diameter and swept area  $A$  are given from the same source and they take the values of 100m and  $7854m^2$  respectively. Another way for swept area's calculation would be the implementation of methodology's part equation 28, since the radius is known and equals with 49m.

Another parameter that is crucial for energy's production estimation is the generator efficiency ( $N_g$ ) and gear box bearing efficiency ( $N_b$ ) which are not given from the manufacture company. Therefore it will be assumed the average value of 97% for  $N_b$  (McGuinn, 2011) and 70% for  $N_g$  (Asis Sarkar, 2012) according to McGuinn and Sarkar papers respectively.

The following figure illustrates the power curve of the selected wind turbine model revealing the fluctuation of the obtained power output respective with the existed wind speed data.

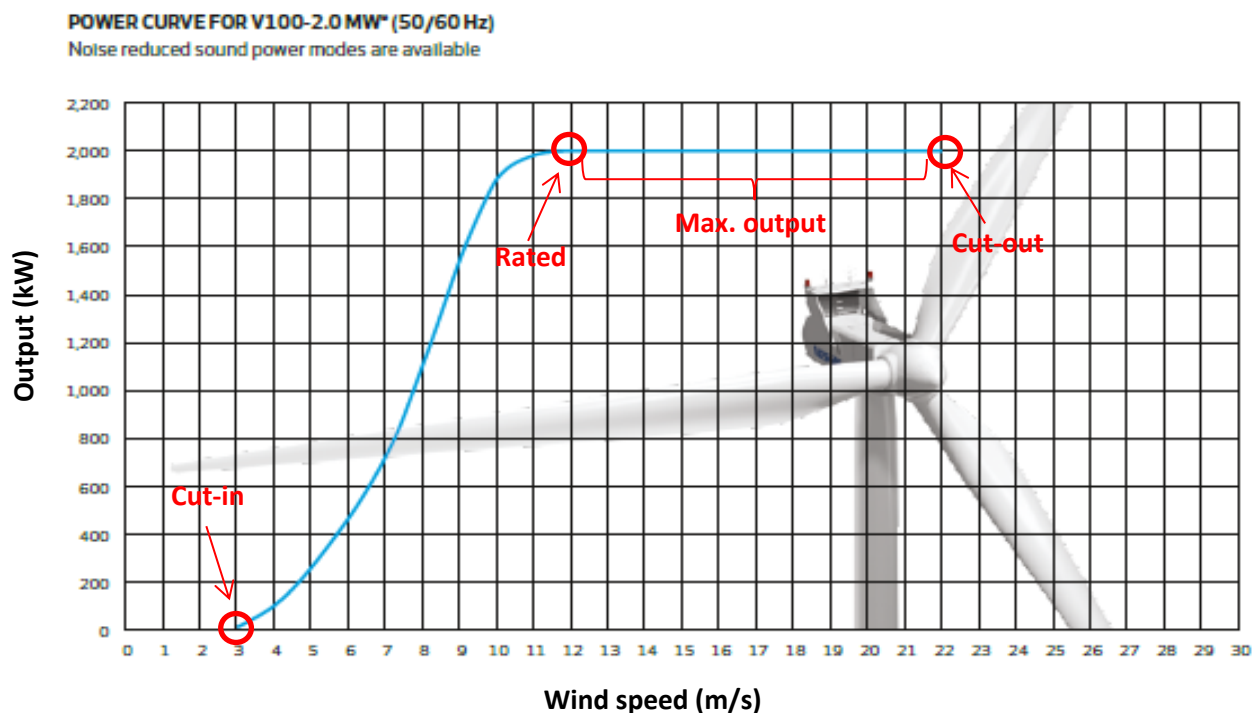


Figure 35: Power curve of Vestas V100-2.0 MW model

On figure 35 the power curve of Vestas V100-2MW is depicted analysing in depth the wind turbine's output production fluctuation relative to the wind speed (Vestas, 2015). For wind currents that vary between 0m/s and 3m/s the turbine remains deactivated. If a continuously linear wind speed increase is assumed then the power curve will reveal an exponential output growth until the rated level of 12m/s. Afterwards the output will remain stable until the wind speed reaches the cut-out point of 22m/s, when the brakes are activated blocking blades movement.

## 8.5. Energy yield produced by the wind system

Since all the technical characteristics of the turbines and the meteorological data of the research location are obtained, the produced energy yield from the installed energy system can be estimated. In this point equation 24 of methodology part will be implemented for the calculation of the produced power in a 10 minute step for the whole year. Moreover, the average 10 minute produced power will be



converted into produced energy taking into account the hours where the turbines were not operating due to extreme low or high wind speeds. The analysis of the generated energy yield will be spited into 3 different parts according to the respective turbine arrays since some wind turbines have reduced energy production due to wake effect formation.

### ➤ 1<sup>st</sup> part: Wind turbines 1-15

Assuming that the prevailing wind direction is from West-South West, then wind turbines 1-15 will not be influenced by any obstacle or turbine sited in front of them that could generate turbulence leading to decreased wind speed and subsequently reduced energy output. Therefore the expected produced monthly energy yield of each wind turbine of them is presented on the following figure 36.

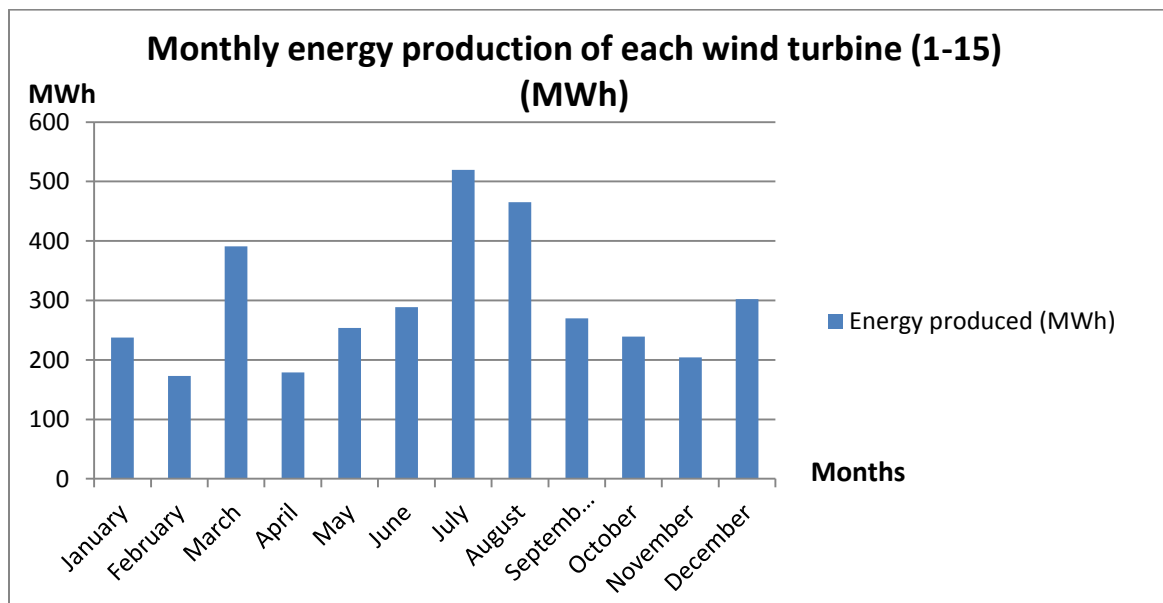


Figure 36: Expected energy produced from wind turbines (1-15)

On figure 36 the expected monthly energy yield produced by **each** wind turbine (1-15) is presented. According to the obtained results the peak months will be July and August reaching the level of 519MWh and 465MWh respectively. March is considered as the third most productive month generating 391MWh followed by December with 302MWh. During the rest of the year the production is significantly decreased varying between 174MWh and 281MWh. The reason of this fluctuation is wind's velocity which reveals increased values during summer months leading to higher energy output. The total yearly energy yield which can be calculated by summing the individual produced energy of each month is **3523MWh**.

### ➤ 2<sup>nd</sup> part: Wind turbines 16-19

These wind turbines are positioned behind another array which is consisted of wind turbines 9-14. In this case the wind that they receive has reduced speed due to wake's effect formation. According to figure 33 where the location of the turbines is depicted, turbine 19 is suffering from turbulent and decreased speed flow created by turbines 11 and 12. Additionally, wind turbine 18 is influenced from



turbines 10 and 11 and wind turbine 17 from 10 and 9 respectively. The reduction level was calculated in section 8.2.2 and it equals with 2.7%. Based on the aforementioned wind speed reduction the produced energy yield is presented on figure 37.

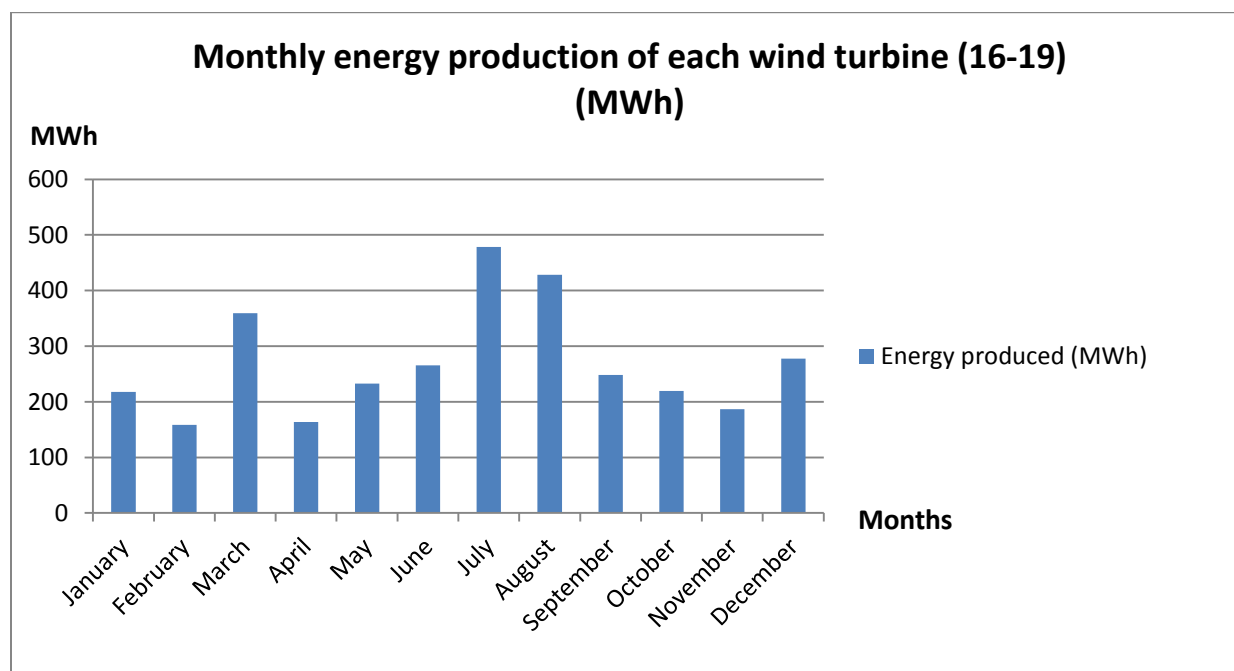


Figure 37: Expected energy produced from each wind turbine (16-19)

On figure 37 the monthly produced energy from the wake affected turbines (16-19) is presented. Observing the schematic it is concluded that graph's fluctuation is similar with the previous one (figure 36), however the monthly production is slightly decreased due to reduced wind speed. The graph illustrates the electricity generation of each wind turbine (16-19) and it shows that during July and August the peak values of 478MWh and 428MWh are reached. The bottom down production months remain February and April producing 158MWh and 164MWh respectively, whereas the total yearly production from each of these wind turbines is expected to be **3236MWh**. The output reduction compared with the no-wake scenario is 8.15%.

### ➤ 3<sup>rd</sup> part: Wind turbines 20-21

Wind turbines 20 and 21 are located behind the wind turbines 15 and 16 (Figure 25). Due to this fact these turbines suffer from output losses due to wake effect development. In this case the decrease of the wind speed was roughly calculated to be around 2.7% in comparison with the wind speed that inserted the blades of turbines 15 and 16 since the vertical distance between them is almost the same as in part 2.

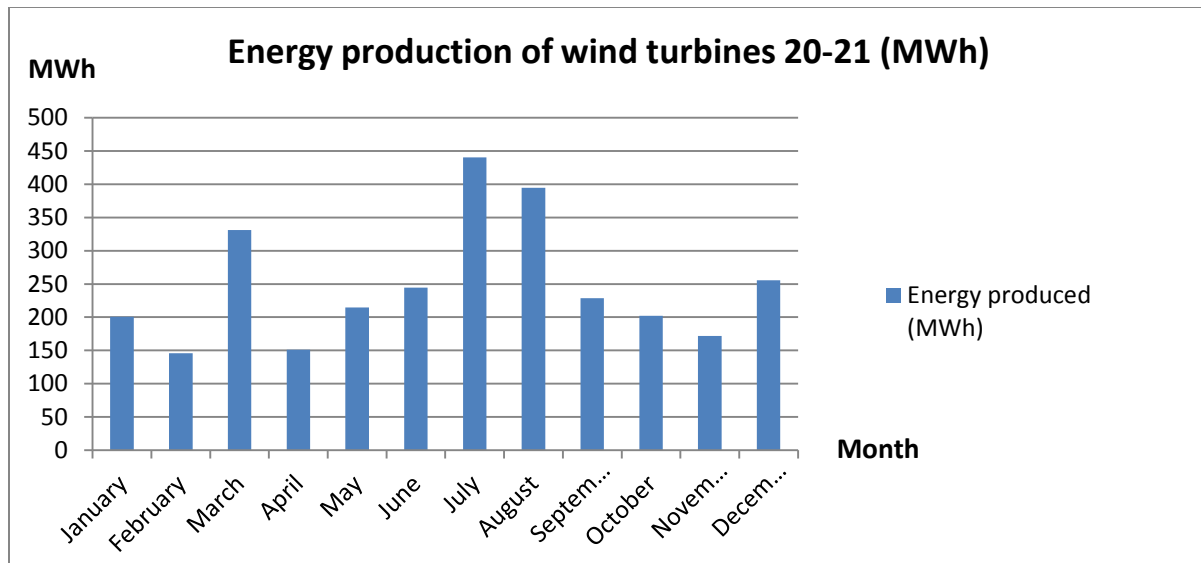


Figure 38: Expected energy produced from wind turbines 20-21

On figure 38 the electricity generation of wind turbine 20 and 21 individually is depicted. According to the obtained results the monthly production of each of these turbines will not overpass the peak value of 440MWh which occurs on July, whereas the total yearly electricity generation is expected to be **2981MWh**. The magnitude of decrease reaches the level of 15.4% compared with the no wake-scenario (turbines 1-15) and the level of 7.9% compared with the turbines 15 and 16.

Based on the above results the total monthly and yearly electricity generation produced by the wind system is estimated and its illustrated on the following graph (Figure 39).

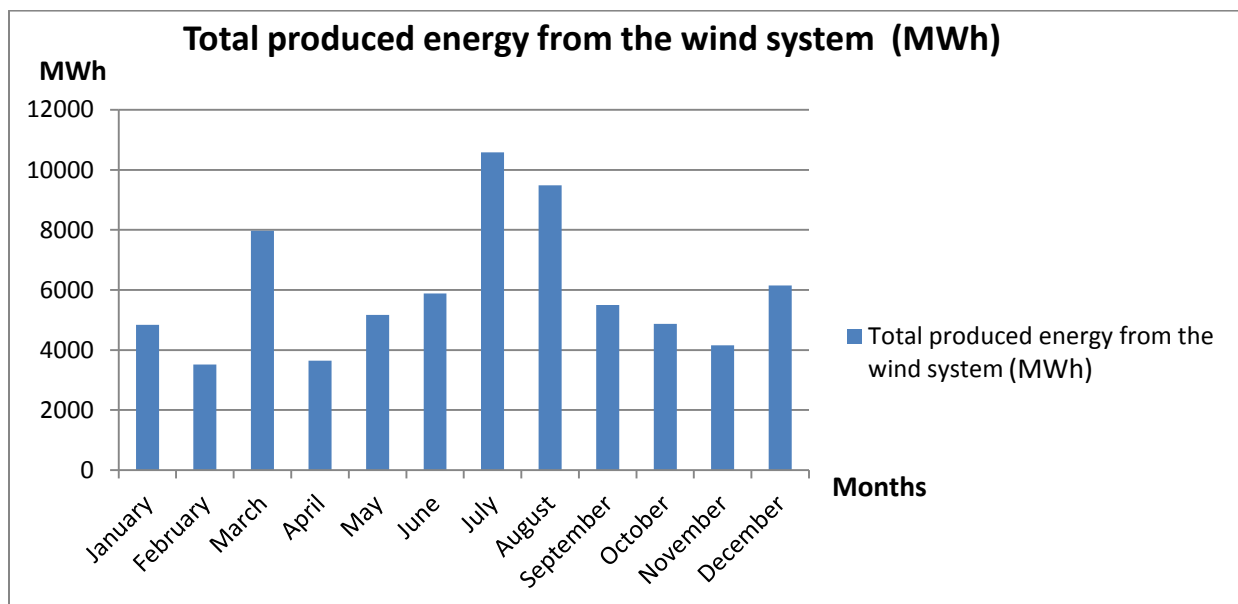


Figure 39: Total energy production from the wind system

Combining all the estimated results of each wind turbine separately, the total monthly produced energy obtained from the wind system was calculated and its depicted on Figure 39. The system which is consisted of 21 wind turbines reaches the peak production on July, generating 10584MWh of electricity. August seems to be the second most productive month reaching the production level of 9484MWh, whereas March follows with 7697MWh. The less productive months are February and April producing only 3518MWh and 3643MWh of electricity respectively. As it was pronounced in previous section the reason why the highest electricity generation occurs on summer is the increased wind dynamic which influences positively the produced energy output of the turbines. The total yearly energy production that can be calculated by summing up the obtained monthly values is expected to be **71748MWh**.

On the following pie (Figure 40) the contribution share of each month to the total yearly energy output is illustrated.

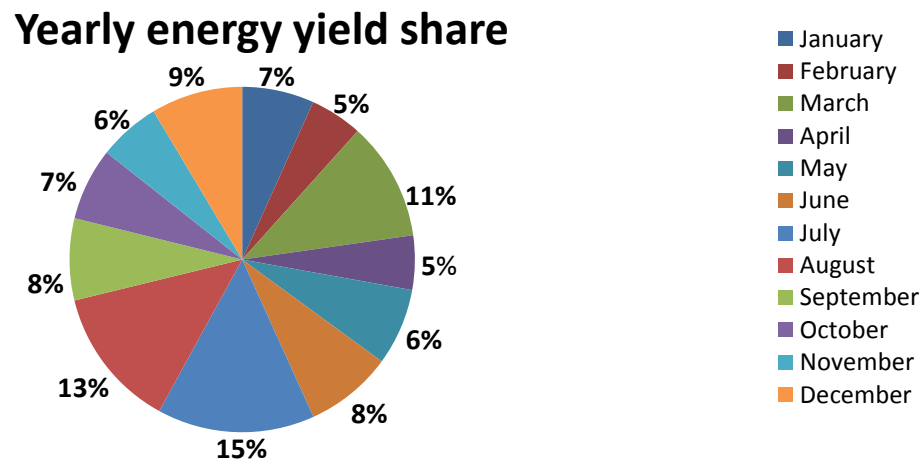


Figure 40: Productivity share of each month

According to figure 40 the highest share of energy belongs to summer period (June-August), when it reaches the value of 36%. Especially during July and August due to increased wind speeds the individual share of these months is 15% and 13% respectively. Thereafter, spring period (March-May) follows with a total participation of 22%. During March the produced energy output is almost equal with the sum of April's and May's output, revealing that the reason why spring comes to the second place is the increased productivity during March. Autumn (September-November) and winter (December-February) participate equally with a share of 21% showing a balanced monthly fluctuation between 5% and 9%. The lowest monthly shares of 5% belong to February and April when the wind speed is decreased to an average of 4m/s.

## 9. Total energy produced from the hybrid system

Since the total yearly and monthly energy produced from the PV and wind system separately is estimated, the total combined energy yield per month produced by the hybrid system can be calculated. The expected monthly production from the PV system will be summed up with the expected monthly



production from the wind system according to sections 7.5 and 8.5. The obtained result can be seen on the following figure 41.

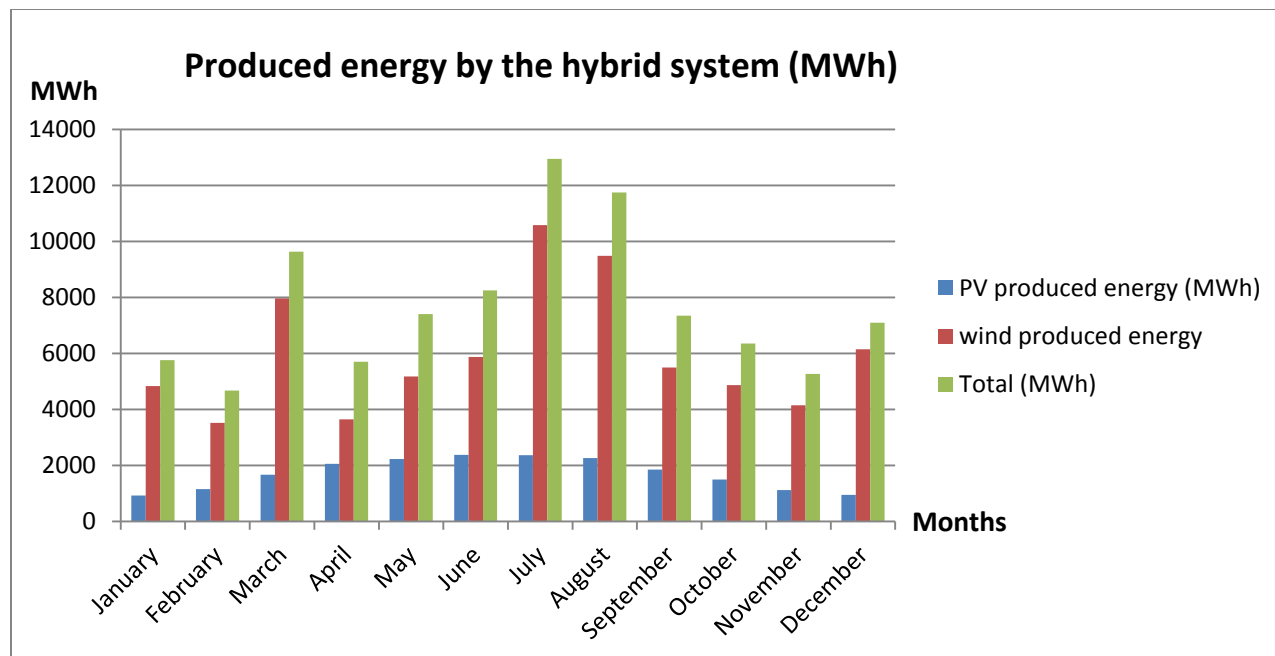
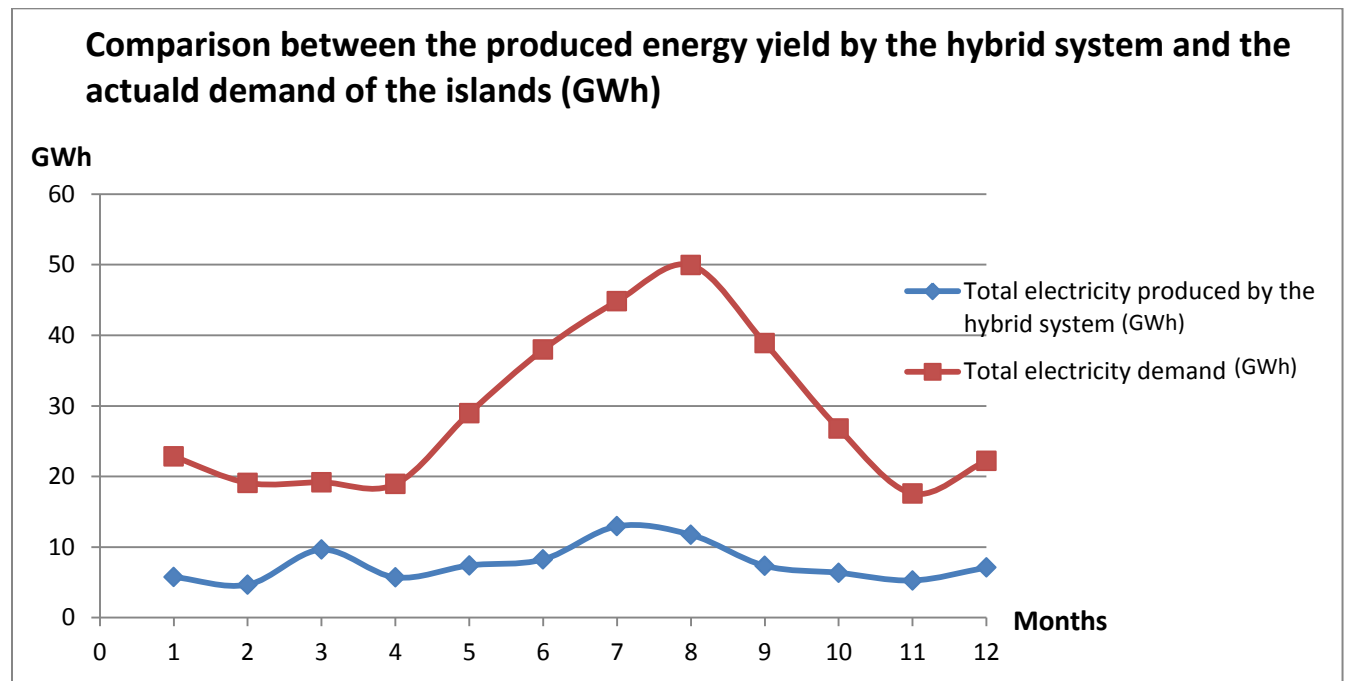


Figure 41: Produced energy yield by the hybrid system

On figure 41 the total electricity production obtained by the hybrid system is presented. The blue colored columns describe the electricity production in MWh from the Photovoltaic installation that took place in Pserimos. On the other hand, the red colored columns represent the wind energy obtained from the 21 wind turbines located on the island. Their fluctuation was analytically described in sections 7.5 and 8.5 respectively. The green columns represent the total electricity production that will be offered for the electricity needs of Cos and Calymnos. According to the graph the electricity production variation is considerably high through the year. During January the production reaches the level of 5763MWh, however February's production is significantly lower. The main reason for that is the light wind dynamic that occurs during February leading to decreased electricity production produced by the wind turbines. Furthermore, March is characterized by an excessive energy yield compared to the previous months reaching the level of 9631MWh, increased by 46.5%. Afterwards a steep decrease is noticed during April, when the hybrid system's electricity generation goes down to 5703MWh. The following months a slight steady increase is presented reaching the peak years value of 12943MWh on July. Furthermore, August seems to be the second most productive month after July generating 11741MWh, followed by March and December with 9631MWh and 7097MWh respectively. During autumn the production fluctuates between 7349MWh and 5269MWh, revealing an average monthly production of 6325MWh. The total yearly electricity production generated by the hybrid system is expected to be **92176MWh or 92.18GWh**.

## 10. Participation share of the hybrid system in the actual electricity consumption of Cos and Calymnos



**Figure 42: Comparison of the actual electricity demand of Cos and Calymnos with the electricity produced by the hybrid system**

By comparing the electricity needs of Cos and Calymnos on a monthly base with the generated electricity obtained from the hybrid system located on Pserimos the following conclusions can be made.

During January the demand of both islands reaches the level of 22.82GWh whereas the participation of the hybrid system is 5.76GWh, covering the 25.3% of the total needs. On February the electricity consumption is slightly decreased dropping down to 19.1GWh, however the electricity generation is also decreased almost by 20% compared with January's production generating 4,67GWh. The participation share during February is 24.45%. Furthermore, March is considered as high electricity participation month, due to the fact that the favorable wind and solar dynamic resulted in the production of 9.63GWh when the demands are not overwhelming the level of 19.2GWh leading to a contribution share of 50.2%. On April the consumption level remains almost stable, whereas the hybrid system's production decreases dropping down to February's level. The participation share of April is 30.1%. From May to August a vertical increase of electricity consumption is noticed, signifying the beginning of the touristic period. Observing the graph's fluctuation between these months the demand varies from 28.96GWh (May) to 49.93GWh (August), which constitutes years peak. The participation share of Pserimos installation as far as May, June, July and August is considered is 25.56%, 21.73%, 28.87% and 23.51% respectively. September is characterized by decreased electricity demand compared to the summer period since the fluency of people arriving on the islands for their summer vacations ends. During September the demand goes down to 38.9GWh and the contribution share becomes 18.9%. As months

pass by and winter approaches the demand decreases even more reaching years top down value of 11.17GWh on November. The contribution of the system in the electricity needs during October and November is 23.74% and 29.94% respectively. The last month of the year presents a consumption growth compared to November reaching the level of 22.22GWh, whereas the electricity production from the hybrid system is expected to be 6.56GWh. December's participation share is calculated to be 29.93%. The average yearly contribution share of the hybrid system is expected to be 27.85%.

## 11. Conclusions

From the above research it was concluded that the success of a PV-Wind hybrid system installation in an island is highly dependent on the wind and solar dynamic of the location. The obtained conclusions from the wind and the PV part will be separately discussed.

- **Cos and Calymnos electricity consumption conclusions**

- The annual consumption needs of both islands based on 2013 and 2014 data is 348.6GWh, whereas the most consuming months are July and August with 45GWh and 48.2GWh respectively.

- **PV park conclusions**

- The average irradiation level per month that is received from the tilted PV surface is  $177.16\text{kWh}/\text{m}^2$ , whereas the peak is achieved on June, when the irradiation level reached the amount of  $248.52\text{kWh}/\text{m}^2$ . Summer is characterized as the most productive period due increased irradiation values.
- The PV panels were installed in the most horizontal part of the island with an incline of  $37^\circ$  and facing to the South.
- The total annual produced electricity obtained by the PV system is 20.43GWh and the monthly mean electricity generation equals with 1.7GWh. The peak production month is June reaching the level of 2.37GWh.
- The average efficiency of the system is 13.9% through the year, however in this case January and December obtain the peak months role with an efficiency of 15.5%.

- **Wind park conclusions**

- In the studied case of Pserimos, the average wind speed among the year was calculated to be 5.14m/s, showing a tend to increase during summer and especially on July and August when the mean speed fluctuated around 7m/s.



- The most prevailing wind direction on the island is West covering the 55% of years total.
- The number of the wind turbines that could be installed on the island is 21, whereas the proper distance with each other for the avoidance of the wake effect is 380m apart perpendicular with the wind direction and 665m apart horizontal to the wind direction. For increased output performance the turbines were sited in between mountains or in the edge of rounded hills taking advantage of the increased wind speed created by the hills and tunnels speed up effects.
- The total produced electricity by the wind system is 71.75GWh, whereas the most efficient month is July when the generation level reaches the amount of 10.58GWh, which is the 15% of the annual production.
- **Hybrid system conclusions**
  - The annual electricity production generated by the hybrid system is expected to be around 92.18GWh covering the 27.85% of the total demand and the monthly mean is 7.68GWh.
  - The most productive season is the summer due to increased irradiation and wind speed levels, whereas the peak is achieved on July when the electricity production reaches 12.94GWh.

## 12. Recommendations

In this project the replacement of oil fueled power plants with a PV-Wind hybrid system for electricity generation was examined and the results revealed that at least at this moment it is impossible to completely substitute petroleum with renewables. Even if the contribution of the system meets the expected demand its very risky to depend on the variable parameter of the weather.

However, the irradiation and wind dynamic that occurs on the majority of the islands characterizes them as very attractive locations for renewables establishment. The development of renewables in off grid locations (islands) will reduce the dependency of the locals from petroleum imports and it will contribute to the turn towards to sustainability.

Moreover, the renewables legislation needs to become friendlier and the bureaucracy should be remodeled, targeting to attract more people that want to invest on this field. Furthermore, the subsidies should come again to the forefront intriguing the possible investors, since financially the idea of investing in renewables seems like a huge burden to the most.

## Bibliography

- A.A. El-Sebaili, F. A.-H.-G. (2009). Global, direct and diffuse solar radiation on horizontal and tilted surfaces. *Applied Energy*, 568-576.
- Asis Sarkar, D. K. (2012). Wind turbine blade efficiency and power calculation with electrical analogy. *International Journal of Scientific and Research Publications*.
- calymnos.gr. (2015). Retrieved from municipality of calymnos: <http://www.kalymnos-isl.gr/en>
- CANMET. (2001-2004). *Photovoltaic project analysis*. Varennes: Minister of natural resources Canada.
- Clive Best, E. v. (2005). *Solar radiation Sata (SODA)*. Retrieved from Solar radiation Sata (SODA): [http://www.soda-is.com/eng/about/about\\_us.html](http://www.soda-is.com/eng/about/about_us.html)
- cos.gr. (2015). *Municipality of Cos*. Retrieved 2015, from [www.cos.gr](http://www.cos.gr): <http://www.kos.gr/el/SitePages/map.aspx>
- econews.gr. (2015). *Wind and Pv installations reaching 20% in the non-grid connected islands*. Athens.
- F.Gonzalez-Logatt. (2012). Wake effect in wind farm performance: Steady-state and dynamic behavior. *Renewable Energy*, 329-338.
- Giannikos. (2015, April 20). Electricity production in Kos and Kalymnos. (K. Stelios, Interviewer)
- Google Earth, E. (2015). *Google earth*. Retrieved from Google earth: <https://www.google.com/earth/>
- Greek tourist organisation, 2. (2014). *Greek islands*. Retrieved from [http://www.visitgreece.gr/en/greek\\_islands](http://www.visitgreece.gr/en/greek_islands): [http://www.visitgreece.gr/en/greek\\_islands](http://www.visitgreece.gr/en/greek_islands)
- ICAP. (2014). *The situation and the future potentials of renewables in Greece*. Athens: ICAP.
- Ioannis Fyrippis, P. A. (2010). Wind energy potential assessment in Naxos Island, Greece. *Applied Energy*, 577-586.
- Katsaprakakis, D. (2007). *Sun Geometry*. Creta: Technological Institution of Creta.
- Katsaprakakis, D. (2007). Wind energy. In K. Dimitris, *Renewables*. Crete: Technological educational institution of Crete.
- Kyritsis. (2015). *deddie Cos*. Retrieved from Operation and managing of Greek electricity grid: <http://www.deddie.gr/el/i-etairaia/organogramma-deddie/deddie/dieuthunsi-perifereias-nisiwn-dpn-perioxi-kw>





- Libii, J. N. (2013). Comparing the calculated coefficients of performance of a class of wind turbines that produce power 330kW and 7500kW. *World transactions of Engineering and Technology Education*.
- M.Ragheb. (2015). *Orography and wind turbine sitting*. Technology review.
- McGuinn, J. (2011). *Wind Turbines: Clean eregy but energy efficient?* Chemntiz, Germany: geartechnology.com.
- meteo.gr. (2015). *Meteorological forecasts of Greece*. Retrieved from meteo.gr:  
<http://meteo.gr/meteoplus/index.cfm>
- Mihalakou, P. (2002). Application of renewable energy sources in the Greek islands of the South Aegean Sea. *Renewable Energy*, 1-19.
- noa.gr. (2015). *Temperature data for the years of 2013 and 2014*. Penteli-Athens: Athens national observatory.
- Nuria Novas Castellano, J. A.-G.-A. (2015). Optimal displacement of photovoltaic array's rows using a novel shading model. *Applied Energy*, 1-9.
- Papadopoulos, P. (2015, June 16). Hybrid system installation. (S. Karatzas, Interviewer)
- Pardalos, R. P. (2013). Layout optimization problem. *Handbook of wind power systems*.
- Ravinder Kumar, L. U. (2005). Estimation of global radiation using clearness index model for sizing photovoltaic system. *Renewable Energy*, 2221-2233.
- Shahnawaz Farhan Khahro, K. T. (2014). Evaluation of solar energy resources by establishing empirical models for diffuse solar radiation on tilted surface and analysis for optimum tilt angle for a prospective location in southern region of Sindh, Pakistan. *Electrical power and energy systems*, 1073-1080.
- SMA-hellas.com. (2015). *SMA Solar Technology*. Retrieved from SMA Solar Technology:  
<http://www.sma-hellas.com/>
- soda-is.com. (2005). *Solar radiation data*. Retrieved from <http://www.soda-is.com/>
- statista.com. (2015). *statista.com*. Retrieved from statista 2015:  
<http://www.statista.com/statistics/263905/evolution-of-the-hub-height-of-german-wind-turbines/>
- Sunovation. (2015). *Sunovation panel technical characteristics*.
- Terabit. (2014). *Submarine telecom industry report*. Massachusette: Terrabit.



Touma, J. S. (2012). Dependence of the Wind Profile Power Law on Stability for Various Locations. . *Air pollution control association*, 863-866.

Tsakiris, F. R. (2010). *Energy development in the Non-Connected Islands of the Aegean Sea*. Reykjavik: National Energy Authority.

Vestas. (2015). *Vestas 2MW Platform*. Vestas.

windustry.org. (2014). Retrieved from <http://www.windustry.org/>

ypeka.gr. (2015). *Ministry of productivity, environment and energy*. Retrieved from Ministry of productivity, environment and energy: <http://www.ypeka.gr/>



## Appendix A- Sun's declination

The obtained declination of the sun for every day of the year was obtained with the use of Coopers equation 9. The declination angle, denoted by  $\delta$ , varies seasonally due to the tilt of the Earth on its axis of rotation and the rotation of the Earth around the sun. If the Earth was not tilted on its axis of rotation, the declination would always be  $0^\circ$ , however Earth is tilted by  $23.45^\circ$  and the declination angle varies plus or minus this amount. Only at the spring and fall equinoxes is the declination angle equal to  $0^\circ$ .

n(days)	$\delta$	n(days)	$\delta$	n(days)	$\delta$	n(days)	$\delta$	n(days)	$\delta$	n(days)	$\delta$	n(days)	$\delta$	n(days)	$\delta$	n(days)	$\delta$
1	-23,01	41	-14,90	81	0,00	121	14,90	161	23,01	201	20,64	241	8,86	281	-6,96	321	-19,60
2	-22,93	42	-14,59	82	0,40	122	15,21	162	23,09	202	20,44	242	8,48	282	-7,34	322	-19,82
3	-22,84	43	-14,27	83	0,81	123	15,52	163	23,15	203	20,24	243	8,10	283	-7,72	323	-20,03
4	-22,75	44	-13,95	84	1,21	124	15,82	164	23,21	204	20,03	244	7,72	284	-8,10	324	-20,24
5	-22,65	45	-13,62	85	1,61	125	16,11	165	23,27	205	19,82	245	7,34	285	-8,48	325	-20,44
6	-22,54	46	-13,29	86	2,02	126	16,40	166	23,31	206	19,60	246	6,96	286	-8,86	326	-20,64
7	-22,42	47	-12,95	87	2,42	127	16,69	167	23,35	207	19,38	247	6,57	287	-9,23	327	-20,82
8	-22,30	48	-12,62	88	2,82	128	16,97	168	23,39	208	19,15	248	6,18	288	-9,60	328	-21,01
9	-22,17	49	-12,27	89	3,22	129	17,25	169	23,41	209	18,91	249	5,79	289	-9,97	329	-21,18
10	-22,04	50	-11,93	90	3,62	130	17,52	170	23,43	210	18,67	250	5,40	290	-10,33	330	-21,35
11	-21,90	51	-11,58	91	4,02	131	17,78	171	23,44	211	18,42	251	5,01	291	-10,69	331	-21,52
12	-21,75	52	-11,23	92	4,41	132	18,04	172	23,45	212	18,17	252	4,61	292	-11,05	332	-21,67
13	-21,60	53	-10,87	93	4,81	133	18,30	173	23,45	213	17,91	253	4,22	293	-11,40	333	-21,83
14	-21,44	54	-10,51	94	5,20	134	18,55	174	23,44	214	17,65	254	3,82	294	-11,75	334	-21,97
15	-21,27	55	-10,15	95	5,60	135	18,79	175	23,42	215	17,38	255	3,42	295	-12,10	335	-22,11
16	-21,10	56	-9,78	96	5,99	136	19,03	176	23,40	216	17,11	256	3,02	296	-12,45	336	-22,24
17	-20,92	57	-9,41	97	6,38	137	19,26	177	23,37	217	16,83	257	2,62	297	-12,79	337	-22,36
18	-20,73	58	-9,04	98	6,76	138	19,49	178	23,34	218	16,55	258	2,22	298	-13,12	338	-22,48
19	-20,54	59	-8,67	99	7,15	139	19,71	179	23,29	219	16,26	259	1,81	299	-13,45	339	-22,59
20	-20,34	60	-8,29	100	7,53	140	19,93	180	23,24	220	15,96	260	1,41	300	-13,78	340	-22,70
21	-20,14	61	-7,91	101	7,91	141	20,14	181	23,18	221	15,67	261	1,01	301	-14,11	341	-22,80
22	-19,93	62	-7,53	102	8,29	142	20,34	182	23,12	222	15,36	262	0,61	302	-14,43	342	-22,89
23	-19,71	63	-7,15	103	8,67	143	20,54	183	23,05	223	15,06	263	0,20	303	-14,74	343	-22,97
24	-19,49	64	-6,76	104	9,04	144	20,73	184	22,97	224	14,74	264	-0,20	304	-15,06	344	-23,05
25	-19,26	65	-6,38	105	9,41	145	20,92	185	22,89	225	14,43	265	-0,61	305	-15,36	345	-23,12
26	-19,03	66	-5,99	106	9,78	146	21,10	186	22,80	226	14,11	266	-1,01	306	-15,67	346	-23,18
27	-18,79	67	-5,60	107	10,15	147	21,27	187	22,70	227	13,78	267	-1,41	307	-15,96	347	-23,24
28	-18,55	68	-5,20	108	10,51	148	21,44	188	22,59	228	13,45	268	-1,81	308	-16,26	348	-23,29
29	-18,30	69	-4,81	109	10,87	149	21,60	189	22,48	229	13,12	269	-2,22	309	-16,55	349	-23,34
30	-18,04	70	-4,41	110	11,23	150	21,75	190	22,36	230	12,79	270	-2,62	310	-16,83	350	-23,37
31	-17,78	71	-4,02	111	11,58	151	21,90	191	22,24	231	12,45	271	-3,02	311	-17,11	351	-23,40
32	-17,52	72	-3,62	112	11,93	152	22,04	192	22,11	232	12,10	272	-3,42	312	-17,38	352	-23,42
33	-17,25	73	-3,22	113	12,27	153	22,17	193	21,97	233	11,75	273	-3,82	313	-17,65	353	-23,44
34	-16,97	74	-2,82	114	12,62	154	22,30	194	21,83	234	11,40	274	-4,22	314	-17,91	354	-23,45
35	-16,69	75	-2,42	115	12,95	155	22,42	195	21,67	235	11,05	275	-4,61	315	-18,17	355	-23,45
36	-16,40	76	-2,02	116	13,29	156	22,54	196	21,52	236	10,69	276	-5,01	316	-18,42	356	-23,44
37	-16,11	77	-1,61	117	13,62	157	22,65	197	21,35	237	10,33	277	-5,40	317	-18,67	357	-23,43
38	-15,82	78	-1,21	118	13,95	158	22,75	198	21,18	238	9,97	278	-5,79	318	-18,91	358	-23,41
39	-15,52	79	-0,81	119	14,27	159	22,84	199	21,01	239	9,60	279	-6,18	319	-19,15	359	-23,39
40	-15,21	80	-0,40	120	14,59	160	22,93	200	20,82	240	9,23	280	-6,57	320	-19,38	360	-23,35
																361	-23,31
																362	-23,27
																363	-23,21
																364	-23,15
																365	-23,09

Table 13: Declination per day